Stable isoporphyrin copolymer: Electrochemical mechanism and behavior and photovoltaic properties

Moussa Boudiaf, Yiming Liang, Raphaël Lamare, Jean Weiss, Helen Ibrahim, Michel Goldmann, Embarek Bentouhami, Vasilica-Adriana Badets, Sylvie Choua, Nolwenn Le Breton, et al.

Stable isoporphyrin copolymer: electrochemical mechanism and behavior and photovoltaic properties

Moussa Boudiaf,[abc,‡] Yiming Liang,[a,‡] Raphaël Lamare,[a] Jean Weiss,[a] Helen Ibrahim,[c] Michel Goldmann,[cd] Embarek Bentouhami,[b] Vasilica Badets,[a] Sylvie Choua,[a] Nolwenn Le Breton,[a] Antoine Bonnefont,[a] and Laurent Ruhlmann,*[a]

[a] Université de Strasbourg, Institut de Chimie, UMR CNRS 7177, 4 rue Blaise Pascal, CS 90032, 67081 Strasbourg cedex, France. E-mail: lruhlmann@unistra.fr
[b] Laboratoire de Chimie, Ingénierie Moléculaire et Nanostructures Université Sétif 1.
Département de génie des procédés faculté de technologie université EL OUED.
[c] Institut des NanoSciences de Paris, UMR CNRS 7588, Sorbonne Université, 4 place Jussieu, boîte courrier 840, F - 75252 Paris, France.
[d] Université Paris Descartes, 45 rue des Saints Pères, F - 75006 Paris, France.

‡ Both authors contributed equally to this work.

† Electronic supplementary information (ESI) available: experimental details, electrochemistry, EQCM, UV-Vis-IR spectra, ESR, XPS, AFM, EIS, and photoelectrochemical responses. (Figs. S1–S21). See DOI:

Graphical Abstract

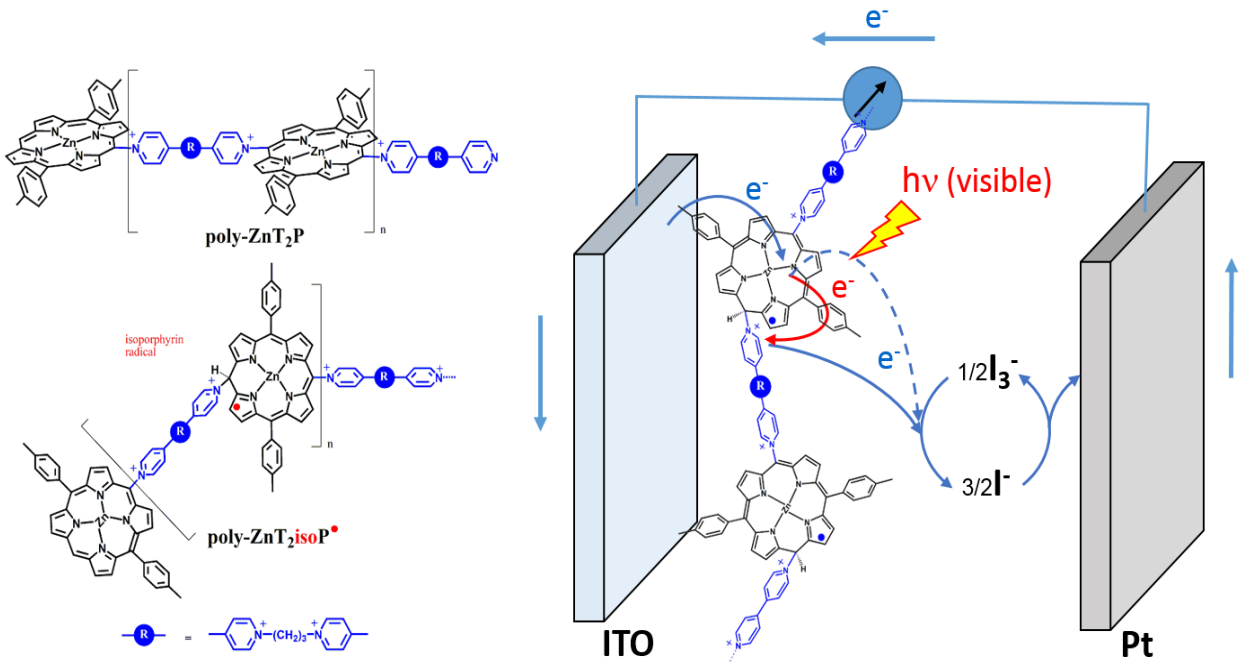

Electro-oxidation of zinc-5,15-bis(*p*-tolyl)porphyrin in the presence of dipyridyl ligand led to the formation of copolymers containing stable isoporphyrin radicals or porphyrins depending on the applied upper potential limit (1.0 V *versus* 1.6 V). The electrochemical properties as well as the photovoltaic performances have been investigated. The photocurrent generation was significantly improved in the case of the isoporphyrin radical copolymer.

Abstract

Two types of porphyrin copolymer thin films were obtained by electropolymerization of zinc-5,15-bis(*p*-tolyl)porphyrin. Electrogenerated porphyrin radical cation and dication are powerful electrophiles which can rapidly react with 1,1''-(1,3-propanediyl)bis-4,4'-bipyridinium hexafluorophosphate salt ($bpy^{+}–(CH_2)_3–^{+}bpy·2PF_6^{-}$) as nucleophiles to form copolymers containing stable isoporphyrin radicals or porphyrins, depending of the applied upper potential limit (1.0 V *versus* 1.6 V). Electrochemical routes leading to these electroactive copolymers are discussed and the unusual redox properties of copolymers containing stable isoporphyrin radicals are studied. The electropolymerization of the two copolymers was monitored by electrochemical quartz crystal microbalance (EQCM). The copolymers were characterized by UV-Vis-NIR spectroscopy, X-ray photoelectron spectroscopy (XPS), electrochemistry, electron spin resonance (ESR) and atomic force microscopy (AFM). Their electrical properties have been studied by electrochemical impedance spectroscopy and their photovoltaic performances have been investigated by photocurrent transient measurements under visible-NIR light irradiation. The isoporphyrin radical copolymer exhibited considerably better photocurrent generation when compared to the porphyrin copolymer.

Keyword: electropolymerization · porphyrinoids · isoporphyrin · pyridinium · viologen · thin films · EPR · EQCM · Impedance · photocurrent generation

1. Introduction

Isoporphyrins are a non-standard tautomeric form of porphyrin, in which one of the *N*-bound protons is shifted to a peripheral *meso*-carbon atom, leading to the loss of aromaticity. Isoporphyrins have been reported as the intermediates in heme oxidation or biosynthesis of chlorophyll [1-2]. In 1960, Woodward [3] hypothesized the formation of isoporphyrin from phlorin by dehydrogenation in the synthesis of chlorophyll[4]. Ten years later, Dolphin *et al* reported the synthesis of the first zinc-isoporphyrin by electrochemical oxidation of zinc-*meso*-tetraphenylporphyrin (ZnTPP) in methanol [5]. More generally, the formation of isoporphyrins results from a nucleophilic attack on an oxidized porphyrin [6-15].

On several occasions, solid state structures have confirmed the molecular structures of isoporphyrin [16-18]. Isoporphyrins show remarkable redox behavior [19-26] and display a characteristic strong absorption in the near-IR ranging from 750 nm to 950 nm suitable for possible applications in photodynamic therapy [27]. A recent review on isoporphyrins details their potential use in medicine, near-IR dyes or photosensitizers, and as model system in biology for natural porphyrin degradation studies, [28] although isoporphyrins have been mostly considered as reaction intermediates, including in previous work by our group.

Our group has shown that π-radical cation porphyrins as well as dications are powerful electrophiles which can rapidly react with nucleophiles to form isoporphyrin intermediates [29]. Most isoporphyrins reported until now show a high tendency to decompose either by ring opening or by rearomatization to regenerate the initial porphyrin. In the case of *β*-octaethyl porphyrins, the corresponding isoporphyrins are not stable, due to the loss of a proton from the saturated *meso*-carbon atom whereas in the case of tetraphenylporphyrin (TPP), the corresponding isoporphyrin is reasonably more stable due to the substitution of the *meso*-carbon atoms by a phenyl group [30-31].

In some cases, stable isoporphyrins can also be obtained by classical synthetic procedures, however, they always result from multistep chemical syntheses which hampers the overall yields of the desired products [32-33]. In this context, electro-generated porphyrin π-radical cations and porphyrin dications, offer a new, alternate and facile synthetic method for obtaining oligo- and poly-porphyrin systems through two possible reaction pathways.

The first pathway consists in the direct coupling of porphyrinic π-radical cation which is mostly effective in the case of 5,15-diarylporphyrins and 5,10,15-triaryl-porphyrins, or when *β* positions bearing protons are not sterically hindered (Scheme 1BD). In the absence of nucleophile, direct *meso–meso, meso–β* or even *β–β* linked dimers of porphyrins can be obtained by electro-oxidation of 5,10,15-triaryl-porphyrins and even longer oligomers were obtained by electrolysis at an applied potential corresponding to the first oxidation of the porphyrin [34]. Furthermore, it was also shown that according depending on the nature of the metal center, *meso–β* linked dimers could be selectively obtained. Magnesium and zinc-5,15-disubstituted porphyrins give exclusively the corresponding *meso–meso* directly linked dimers, whereas copper, palladium, nickel and also free base porphyrins led exclusively to *meso–β* linked dimers [35]. The original yields, lower than 50%, were significantly increased to obtain yields as high as 95% for electrochemical couplings [36].

In an extension of their pioneering studies, Osuka *et al.* also showed that *meso–meso* coupling of zinc-5,15-diaryl-porphyrins leading to oligomers could be achieved selectively in the presence of 1.5 eq. of $AgPF_6$ in $CHCl_3$ containing 0.5% of *N*,*N*-dimethylacetamide [37].

In this context, Lucas, Vorotyntsev and coworkers reported electropolymerization of magnesium porphin (all *meso* or β carbon atoms bearing H), allowing the formation of long chains of porphin connected through direct *meso–meso* links [38-46].

The second reactive pathway is the addition of a nucleophile on the electron deficient porphyrin radical cations or dications which can occur at the "free carbons" (*meso* or β carbon atoms bearing H) of oxidized porphyrin [47-48]. This electro-synthetic method led to the formation of various substituted porphyrins. In particular, bidentate nucleophiles such as the 4,4'-bipyridine [29], dipyridyl ligand [49-52] or diphosphine [53-55] yielded porphyrin dimers or oligo-porphyrins with significant yields.

Lucas and coworkers also investigated electrochemical nucleophilic substitutions on magnesium porphin [56]. In this case, an electro-generation of the porphin radical cation in the presence of pyridine led to the regioselective mono *meso*-substitution of the porphin in 73% yield.

We took advantage of the reactivity of oxidized porphyrins to develop an easy and original method of porphyrin Electropolymerization. We will first describe the possibility to obtain a copolymer of porphyrins with iterative scans by cyclic voltammetry from the mono-substituted 5-ZnOEP(*meso*-bpy)$^+$ porphyrin (ZnOEP = zinc-β-octaethylporphyrin) [57-58]. On the one hand, when the positive potential limit was sufficiently high (*i.e.* allowing the formation of the porphyrin dication 5-ZnOEP^{2+}(*meso*-bpy)$^+$, the current increased progressively, showing the formation of a conducting copolymer film on the working electrode. On the other hand, if the iterative sweeps were stopped at a potential only allowing the formation of the π-radical cation of the porphyrin (5-ZnOEP$^{+\bullet}$(*meso*-bpy)$^+$) no change of the cyclic voltammograms was observed [59] indicating that the electropolymerization did not occur. In this case, the oxidation wave of the porphyrin remained reversible, showing that the electro-generated π-radical cation porphyrin did not react further.

Despite the fact that the formation of radical cation was sufficient to perform mono-substitutions onto macrocycles, the electropolymerization failure can be attributed to the presence of the bulky ethyl groups influencing the reaction kinetics. Without a doubt, the nucleophilic attack on the π-radical cation is slower than the attack on the dication in the case of zinc-β-octaethylporphyrin (**ZnOEP**).

Accordingly, if the characteristic time of the potential scan during the electropolymerization is shorter than that of the nucleophilic attacks onto the π-radical cation porphyrin, the substitution will not occur and the radical cation will be reduced during the cathodic scan. An $E_1(E_2C_{Nmeso}E_3C_B)_n$ mechanism has been proposed in the case of 5-ZnOEP(*meso*-bpy)$^+$ porphyrin where the double-oxidation step at the beginning (steps E_1E_{2n}) allows the electro-generation of the dication porphyrin and then the copolymer formation [57-58].

We have also developed the easy electropolymerization of porphyrins with the direct use of commercial and unsubstituted **ZnOEP** porphyrin, in the presence of 4,4'-bipyridine. The growth of the copolymer was obtained only if the porphyrin dication was generated in the presence of 4,4'-bipyridine.

In this work, a new strategy led to the formation of stable isoporphyrins integrated in the copolymers. It is shown that stable isoporphyrins copolymers can be obtained during porphyrin oxidation when sterically less hindered porphyrin is used, such as the zinc-*meso*-5,15-ditolyl-porphyrin (**ZnT$_2$P**) which presents only two *meso* positions occupied by one substitutable proton at positions C10 and C20 (Scheme 1). These new copolymers containing stable isoporphyrins will be described and compared with the "classical" porphyrin copolymer prepared using the strategy developed in our group [52,60].

The characteristic strong absorption of isoporphyrins in the near-IR region is also promising for the development of develop near-IR dyes or photosensitizers for photovoltaic devices and the photocurrent generation.

The formation of such type of stable isoporphyrin copolymer will be achieved by oxidation of porphyrin such as zinc-5,15-ditolyl-porphyrin (**ZnT$_2$P**) in the presence of dipyridyl ligand. Copolymers containing isoporphyrin radical (**poly-ZnT$_2$isoP$^\bullet$**) or porphyrin (**poly-ZnT$_2$P**) depending of the upper potential limit (1.0 V *versus* 1.6 V) of the iterative potential cycles (Fig. 1) will be obtained. The 1,1''-(1,3-propanediyl)bis-4,4'-bipyridinium hexafluorophosphate salt ($bpy^+–(CH_2)_3–^+bpy\cdot 2PF_6^-$) was used for this study.

The formation of these copolymers on ITO electrode has been monitored in-situ by Electrochemical Quartz Microbalance (EQCM). The two copolymers were also characterized UV-Vis-NIR spectroscopy, X-ray photoelectron spectroscopy, electrochemistry, ESR (Electron Spin Resonance), AFM and electrochemical impedance spectroscopy (EIS). The photocurrent generation has been

investigated under visible light illumination and the performances of **poly-ZnT$_2$isoP$^\bullet$** and **poly-ZnT$_2$P** copolymer thin films are compared.

2. Experimental

2.1. Materials. All solvents were of reagent grade quality and used without further purification. Zinc-*β*-octaethylporphyrin (**ZnOEP**) was purchased from Sigma-Aldrich and used without further purification. The 1,1''-(1,3-propanediyl)bis-4,4'-bipyridinium hexafluorophosphate salt ($bpy^+–(CH_2)_3–{}^+bpy\cdot 2PF_6^-$) was synthesized according to procedures described in literature [61-62].

2.2. Synthesis of ZnT2P and ZnAT2P.

2.2.1. ZnT$_2$P.

The free base 5,15-bis(p-tolyl)porphyrin (**H$_2$T$_2$P**) [63-65] was synthetized according to published procedures from 2,2'-dipyrromethane and *p*-tolualdehyde [66]. The free base was then metallated with $Zn(OAc)_2$ in THF to give zinc-5,15-bis(p-tolyl)porphyrin (**ZnT$_2$P**).

2.2.2. ZnAT$_2$P.

Free-base porphyrin 5-(4-methoxyphenyl)-10,20-di-*p*-tolylporphyrin [67] was prepared by literature procedures and subsequently metallated (288 mg, 0.48 mmol, 1 eq) in THF using zinc acetate $Zn(OAc)_2$ (1059 mg, 4.8 mmol, 10 eq). The solution was refluxed for 1h. The crude product was purified by silica gel column chromatography with dichloromethane/cyclohexane (3/7) to afford 5-(4-methoxyphenyl)-10,20-di-p-tolylporphyrin zinc **ZnAT$_2$P** (294 mg, 0.45 mmol, 93%) as purple solid.

^{1}H NMR (400 MHz, $CHCl_3$-d, 25°C): δ 10.20 (s, 1H, H *meso*), 9.37 (d, J = 4.5 Hz, 2H, H pyrr.), 9.10 (d, J = 4.5 Hz, 2H, H pyrr.), 9.01 (m, 4H, H pyrr.), 8.12 (d, J = 7.8 Hz, 6H, $H_{o\text{-anis}}$ + $H_{o\text{-tolyl}}$), 7.58 (d, J = 7.6 Hz, 4H, $H_{m\text{-tolyl}}$), 7.28 (d, J = 7.8 Hz, 2H, $H_{m\text{-anis}}$), 4.09 (s, 3H, OCH_3), 2.73 (s, 6H, CH_3) ppm (Fig. S1).

^{13}C NMR (125 MHz, $CHCl_3$-d, 25°C): δ 159.37, 150.47, 150.43, 150.28, 150.01, 139.95, 137.29, 135.59 (CH), 134.68 (CH), 132.83 (CH), 132.14 (CH), 132.02 (CH), 131.77 (CH), 127.55 (CH), 120.82, 112.17 (CH), 105.85 (CH), 55.77 (CH_3), 21.77 (CH_3) ppm (Fig. S2).

UV-Vis: λ= 419, 547, 587 nm.

ESI-TOF: *m/z* = 658.17. Calcd for $C_{41}H_{30}N_4OZn$ ([M^+]): 658.17.

TLC (silica): R_f: 0.33 (cyclohexane/dichloromethane, 50/50).

2.3. Electrochemistry and photoelectrochemistry. Voltammetric and electrochemical impedance measurements have been performed with a standard three-electrode system using a PARSTAT 2273 potentiostat. Glassy carbon or *single-side coated* indium-tin-oxide (ITO, SOLEMS, 25-35 Ω/cm^{-2}) plates, with a surface of about 1 cm^2 have been used as working electrodes. A platinum wire has been used as auxiliary electrode. The reference electrode was a saturated calomel electrode (SCE). It was electrically connected to the solution by a junction bridge filled with the electrolyte. Photoelectrochemical responses of the films were measured by illumination of the electrode using a 300 W Xe arc lamp (with $\lambda > 385$ nm long pass filter). A Pt wire is used as counter and reference electrode. The measurements were performed in water containing 5 $mmol.L^{-1}$ of I_2 and 0.5 $mol.L^{-1}$ of NaI. In solution I_2 reacts with I^- to give I_3^-. I_3^- and I^- anions act as reversible redox mediator and also as conducting electrolyte.

2.4. UV-visible-NIR Spectroscopy. UV–vis-NIR absorption spectra of the copolymers deposited on ITO or in DMF solution, as well as the starting monomers, have been recorded using an Agilent 8453 spectrophotometer.

2.5. Electron Spin Resonance spectroscopy. ESR spectra were recorded with an ESP 300E spectrometer (Bruker) operating at X-band and equipped with a high sensitivity resonator (4119HS-W1). Spectra were recorded with 2 mW microwave power, a modulation frequency of 100 kHz and a modulation amplitude of 0.1 mT. Computer simulations of the ESR spectra were performed with the help of easyspin software [68].

2.6. X-ray Photoelectron Spectroscopy (XPS). XPS experiments were carried out using a Thermo VG. Multilab ESCA 3000 spectrometer (Thermo Fisher Scientific, Waltham, MA, USA) equipped with an Mg KR radiation (*h* =1253.6 eV) or Al KR radiation (*h* = 1486.6 eV) source. The energy shift due to electrostatic charging was subtracted using the sp^2 carbon C 1s band at 284.8 eV coming from

the isoporphyrin or porphyrin macrocycle. The data analysis was implemented by using the XPSPEAK4.1 software.

2.7. Synthesis of the poly-ZnT$_2$P. Electropolymerization has been carried out under an argon atmosphere in a 0.1 mol.L^{-1} NBu_4PF_6 CH_3CN/1,2-$C_2H_4Cl_2$ (3/7) solution containing 2.5×10^{-4} mol.L^{-1} of **ZnT$_2$P** or **ZnOEP** and 2.5×10^{-4} mol.L^{-1} of bpy$^+$–$(CH_2)_3$–$^+$bpy·$2PF_6^-$. ITO electrodes, with a surface of 1 cm^2, were used as working electrode.

Electropolymerization has been tested by applying iterative potential scan between -1.00 V and 1.00 V *vs.* SCE with **ZnOEP** in the presence of bpy$^+$–$(CH_2)_3$–$^+$bpy·$2PF_6^-$ but no copolymers and film deposition could be obtained (Fig. 1) as indicated by the absence of modifications in the cyclic voltammograms. The oxidation wave of the porphyrin remains reversible, showing that the electrogenerated π-radical cation porphyrin does not react further.

In contrast, the formation of the copolymer is observed when zinc-5,15-tolyl-porphyrin **(ZnT$_2$P**) is used instead of **ZnOEP** under the same conditions (concentrations, solvent and supporting electrolyte). Electropolymerization occurs during iterative potential scans either between -1.00 V and 1.00 V (just after the first oxidation wave of the porphyrin) *vs.* SCE or between -1.00 V and 1.60 V (after the second oxidation wave of the porphyrin) *vs.* SCE in the presence of bpy$^+$–$(CH_2)_3$–$^+$bpy·$2PF_6^-$ (Scheme 1 and Fig. 2). After electropolymerization, the modified working electrodes were systematically washed with CH_3CN in order to remove traces of the monomers and of the NBu_4PF_6 eventually remaining on the electrodeposited films.

2.8. Electrochemical quartz crystal measurement (EQCM).

A QCA-922 (SEIKO EG&G instrument) system combined with Versa STAT 3 was used for carrying out simultaneous electrochemical quartz crystal (EQCM) and cyclic voltammetric measurements. The electrochemical cell was assembled in a glove box using an ITO AT-cut quartz crystal resonator (mirror finished; resonant frequency, 9.08 MHz ± 50 kHz; A=0.2 cm^2; SEIKO EG&G., LTD) as working electrode, a platinum wire as counter electrode, and an Ag/AgCl wire as a quasi-reference electrode. The solution used here is the same as the one used for electropolymerization of the copolymers on larger ITO electrodes. Iterative potential scans have been performed at a sweep rate of 100 mV s^{-1} at room temperature with simultaneous recording of the quartz resonance frequency.

Changes in the quartz resonance frequency (Δf) have been converted into mass changes (Δm) on the ITO-coated quartz during iterative cycling by applying Sauerbrey's equation (Eq. 1):

$$\Delta f = -2f_0^2.\Delta m/A(\mu\cdot\rho)^{1/2} \qquad \text{(Equation 1)}$$

where f_0 stand for the resonant frequency of the fundamental mode, ρ is the density of the crystal (2.684 $g.cm^{-3}$), A is the working electrode surface (0.2 cm^2) of the ITO quartz crystal resonator, μ is the shear modulus of quartz ($2.947\times10^{11} m^{-1}.s^{-2}$). Sauerbrey's equation (Eq. 1) has been used to calculate Δm considering a rigid and evenly distributed mass on the surface of the resonator.

2.9. Atomic force microscopy (AFM).

Atomic force microscopy (AFM) measurements have been conducted directly on the ITO surfaces using a Dimension 3100 (Veeco) in the tapping mode under ambient conditions. Silicon cantilevers (Veeco probes) with a spring constant of 40 N/m and a resonance frequency in the range of 300 kHz have been used. The scanning rate was 1.0 Hz.

The thickness measurements have been carried out upon scratching the film with a metallic tip. The thickness was then estimated by comparing the height on each side of the scratch.

3. Results and Discussion

3.1. Electropolymerization of zinc-5,15-ditolylporphyrin (ZnT_2P)

The molecular precursors porphyrins zinc-*β*-octaethylporphyrin (**ZnOEP**), zinc-5,15-bis(*p*-tolyl)porphyrin (**ZnT_2P**), as well as dipyridyl ligands, $bpy^+–(CH_2)_3–^+bpy\cdot2PF_6^-$ and close-related compound zinc-5-(4-methoxyphenyl)-10,20-di-p-tolylporphyrin (**$ZnAT_2P$**) are depicted in Scheme 1.

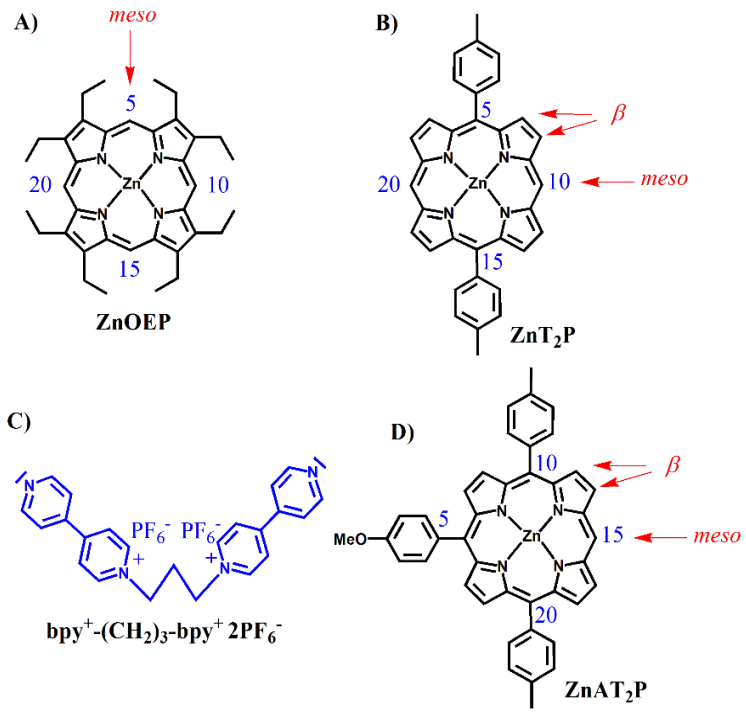

Scheme 1. Representation of A) zinc-*β*-octaethylporphyrin, **ZnOEP**, B) zinc-5,15-bis(*p*-tolyl)porphyrin, **ZnT$_2$P**, C) bpy$^+$–(CH$_2$)$_3$–$^+$bpy·2PF$_6^-$, D) zinc-5-p-anisyl-10,20-bis(p-tolyl)porphyrin (**ZnAT$_2$P**).

The syntheses of the copolymers were achieved *via* our previously reported electropolymerization method [57-58-70]. It relies on the addition of dipyridyl ligands to an electro-generated π-radical cation or dication porphyrin produced by iterative voltammetric scans (Fig. 2).

3.1.1. Reactivity of zinc-*β*-octaethylporphyrin **ZnOEP**

In our previous work, electropolymerization of zinc-*β*-octaethylporphyrin (**ZnOEP**) was carried out at a sufficiently high positive potential value to produce doubly oxidized porphyrins (dication) which are readily reacting with dipyridyl nucleophile to produce copolymers [57-58]. Furthermore, mono-substituted **ZnOEP** porphyrin can also be obtained by electrosynthesis from the mono-oxidized π-radical cations **ZnOEP$^{+\bullet}$** whereas electropolymerization requires the formation of porphyrin dications **ZnOEP^{2+}**, most probably due to kinetic issues (porphyrin dications react more rapidly with pyridyl groups than the radical cation). An E(EC$_{N\ meso}$EC$_B$)$_n$E mechanism has been previously proposed in the case of **ZnOEP** to account for the electropolymerization process where C$_{N\ meso}$ relates to the nucleophilic attack at the *meso* position of the porphyrin to yield an isoporphyrin intermediate [71]. This latter compound is then oxidized (electrochemical step) and the hydrogen atom initially

located on the *meso*-carbon is released (chemical step C_B). The corresponding global reaction is written in Eq. 2 assuming that only the disubstitution on the porphyrin occurs at *meso* positions (Schemes 1-2):

(n+1) ZnP + (n+1) Py-R-Py → ZnP-(Py^+-R-Py^+-ZnP)$_n$-Py^+-R-Py + (2n+1)H^+ + (4n+2)e^- (Equation 2)

(where -R- = py^+-$(CH_2)_3$-py^+ and ZnP = zinc porphyrin)

In the case of **ZnOEP**, the disubstitution occurs at least at two of the four *meso* positions (*cis* or *trans* di-substitution: substitution on the carbons C5 and C10 or C5 and C15 respectively) [71].

In this work, the nucleophile used is bpy^+–$(CH_2)_3$–$^+$bpy·$2PF_6^-$ and the copolymer is obtained in the presence of **ZnOEP** only after generation of the porphyrin dications **ZnOEP**$^{2+}$ by iterative scans (between -1.3 V and 2.0 V) or by potentiostatic electrolysis at sufficiently high potential [52].

In the present work, we have found that when the anodic potential limit is only above the potential at which the radical cation **ZnOEP**$^{+\bullet}$ is generated (i.e. 0.8 V), no film is deposited on the ITO electrode proving that the polymerization doesn't occur in this case (Fig. 1). Moreover, the oxidation wave of the macrocycle remains rather-irreversible showing that the electrogenerated radical cation does not react further. It should be noticed that the reduction wave detected at -0.7 V corresponds to the redox couple bpy^+–$(CH_2)_3$–$^+$bpy/ $bpy^\bullet$–$(CH_2)_3$–$^\bullet$bpy.

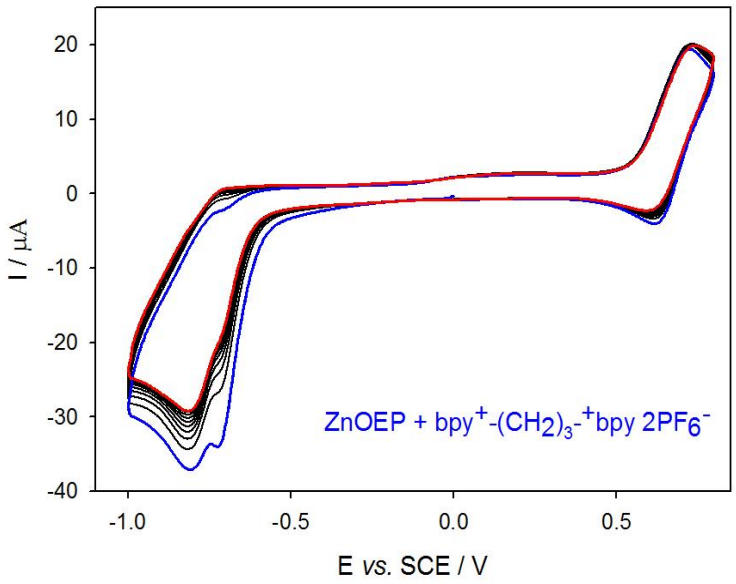

Fig. 1. Cyclic voltammograms recorded during 25 iterative scans conducted between −1.00 V and +0.80 V *vs.* SCE in a 1,2-$C_2H_4Cl_2$/CH_3CN (7/3) solution and NBu_4PF_6 (0.1 mol.L^{-1}) of **ZnOEP** (0.25 mmol L^{-1}) in the presence of bpy^+–$(CH_2)_3$–$^+$bpy $2PF_6^-$ (0.25 mmol L^{-1}). WE: ITO. S = 1 cm^2. *v* = 0.1

V s^{-1}. Blue curve: first scan (n=1). Red curve: final scan (n = 25). (For interpretation of the references to color in this figure legend, the reader is referred to the Web version of this article.)

In our former work, we concluded that, while the formation of radical cation is enough to obtain monosubstituted porphyrins [59,72] *via* electrosynthesis (but necessitating much longer time than cyclic voltammetry), the formation of dication is requested to perform the electropolymerization of **ZnOEP** *via* iterative cyclic voltammetry. A kinetic restraint can explain this difference considering that the nucleophilic attack is faster on the dication than on the radical cation. As a result, if the iterative scans are stopped at a potential allowing only the formation of the radical cation, the characteristic time of the cyclic voltammetry at 100 $mV.s^{-1}$ might be too short for the nucleophilic attack to occur. The presence in this case of the ethyl groups decreases drastically the kinetic of the nucleophilic attack at the *meso* position C5, C10, C15 or C20 respectively. Also, the need to apply a higher potential for electropolymerization is related to the degree of substitution of macrocycles and the presence of two positively charged groups on each porphyrin once included in the copolymers. Consequently, porphyrins are more and more difficult to oxidize resulting in an increase of potential at which the polymerization occurs. This explanation is also supported by the fact that a higher applied potential has always been required to perform electrosynthesis of multi-substituted porphyrins through electrolysis [49,73].

It can also be noted that higher anodic potential limit should lead to longer copolymers chains. Otherwise, if the upper potential is too low, but still higher than that of the first monomer oxidation, only small oligomers should be obtained which may dissolve.

3.1.2. Reactivity of zinc-*meso*-5,15-ditolyl-porphyrin **ZnT$_2$P**

In this study, we have decided to use the zinc-*meso*-5,15-ditolyl-porphyrin (**ZnT$_2$P**) which presents only two *meso* positions occupied by one substitutable proton at positions C10 and C20. Additionally, all the β positions of **ZnT$_2$P** are occupied only by protons. Such porphyrin will provide better accessibility for the nucleophilic attack of the pyridyl groups of $bpy^{+}–(CH_2)_3–^{+}bpy\cdot 2PF_6^{-}$ in comparison to **ZnOEP** (Scheme 1). In the literature, the magnesium porphin showed only the nucleophilic substitution with pyridine or triphenylphosphine at the *meso*-positions even when the β-positions are only occupied by protons [74]. Electrosynthesis of Zn and Mg *meso*-triarylphosphonium

porphyrin were also reported from Zn or Mg 5,10,15-triarylporphyrin showing a nucleophilic substitution mainly at the *meso* and not the *β* position [75]. Furthermore, the electrochemical oxidation of pyridin-2-ylthio-meso substituted Ni(II) porphyrins afforded oxidative C-N fusion of pyridinyl-substituted porphyrins again at the *meso* position giving cationic and dicationic pyridinium-based products [76].

Lastly, in order to demonstrate that the copolymer can be obtained using only **ZnT$_2$P** which presents two *meso* positions bearing H (*i.e.* position 10 and 20, methine bridges), we have synthesized the zinc-5-(4-methoxyphenyl)-10,20-di-p-tolylporphyrin, **ZnAT$_2$P** (Scheme 1) in which one *meso* position (C5) is occupied by a methoxyphenyl group. The experimental protocol for the synthesis of **ZnAT$_2$P** is described in the ESI. In the presence of $bpy^{+}–(CH_2)_3–^{+}bpy\cdot 2PF_6^{-}$ and **ZnAT$_2$P** no copolymer was obtained even after a large number of iterative scans between -1.0 V and 1.0 V ($v = 100\ mVs^{-1}$, Fig. S3) showing that two *meso* positions bearing H are required to form the copolymer. Additionally, for zinc 5,15-ditolyl porphyrin (**ZnT$_2$P**), the nucleophilic attack appears to be allowed only at the 10 as well as the 20 *meso* positions of the porphyrin.

It must be noted that in the absence of nucleophile, the electrogenerated radical **ZnT$_2$P$^{+\bullet}$** may undergo a radical coupling reaction and the formation of one dimer with C-C bond formation through *meso–meso*, *meso–β* or *β–β* link between two macrocycles. Indeed, previous works in the literature using the 5,15-bis(3,5-di-tert-butylphenyl) porphyrin showed only the formation of a mixture of *meso–meso* and *meso–β* linked dimers. These dimers presented a splitting of the Soret band of the optical spectra [77-79].

However, when potential iterative scans are performed between -1.0 V and +1.0 V or +1.6 V using **ZnT$_2$P** alone (in the absence of nucleophile) no film deposition onto the ITO electrode is observed suggesting that the kinetic of radical coupling reaction is relatively slow. The formation of dimer and eventually small oligomer which are soluble cannot be completely excluded.

Additionally, in the presence of $bpy^{+}–(CH_2)_3–^{+}bpy\cdot 2PF_6^{-}$ nucleophile, the radical coupling is still not detected during the iterative scans, copolymers being obtained only with viologen or double viologen. The UV-vis-NIR spectra of the copolymer deposited onto ITO electrode also confirm the absence of dimer **(ZnT$_2$P)$_2$** or oligomer **(ZnT$_2$P)$_n$** through radical coupling in the solid state. The control of the solution after the electropolymerization has been checked by UV-vis-NIR spectroscopy. Only the starting **ZnT$_2$P** monomer could be detected in the solution, even after a large number of

iterative scans, showing the absence of significant quantity of dimer obtained by radical coupling under these conditions. UV-vis-NIR spectroscopy also confirms the absence of demetallation of the starting **ZnT_2P** porphyrin in solution even after deposition of a large number of films. It demonstrates that the Zn metal ion remains in the porphyrin ring during electropolymerization and that there is no **$(ZnT_2P)_2$** dimer or oligomer (formed through radical coupling) in detectable amount.

The general electropolymerization procedure used to deposit the porphyrin-based polymers onto ITO electrode surfaces is described below. This process depends on the polarization of the working electrode during the potential scan that is either at the first oxidation potential to produce **$ZnT_2P^{+\bullet}$** (iteration between -1.0 V and +1.0 V) or at the second oxidation potential to produce **ZnT_2P^{2+}** (iteration between -1.0 V and +1.6 V). It involves a series of intermolecular cascade reactions leading to formation of physisorbed oligomers and copolymers (see Scheme 2 for suggested mechanism). The bridging *bis*-nucleophile used as a precursor is a the dicationic bispyridinium $bpy^+–(CH_2)_3–^+bpy\cdot 2PF_6^-$ offering two terminal pyridine rings (Scheme 1).

All the information summarizing the conditions of the formation of the copolymers, the species present in the starting solution, their concentrations and the anodic potential limit used in oxidation are given in Table 1.

Table 1. Electropolymerization conditions.

Monomer (c = 0.25mM)	Copolymer	Iterative scan (v = 0.1 Vs^{-1}) between:	Solvent and electrolyte
ZnT_2P + $bpy^+–(CH_2)_3–^+bpy\cdot 2PF_6^-$	**poly-ZnT_2isoP$^\bullet$**	-1.00 V and +1.00 V	1,2-$C_2H_4Cl_2$ /CH_3CN (7/3) solution + 0.1 M $TBAPF_6$
ZnT_2P + $bpy^+–(CH_2)_3–^+bpy\cdot 2PF_6^-$	**poly-ZnT_2P**	-1.00 V and +1.60 V	
ZnOEP + $bpy^+–(CH_2)_3–^+bpy\cdot 2PF_6^-$	**No reaction**	-1.00 V and +1.00 V	
ZnOEP + $bpy^+–(CH_2)_3–^+bpy\cdot 2PF_6^-$	**poly-ZnOEP**[a]	-1.00 V and +1.60 V	

[a] copolymer already published, see reference 57.

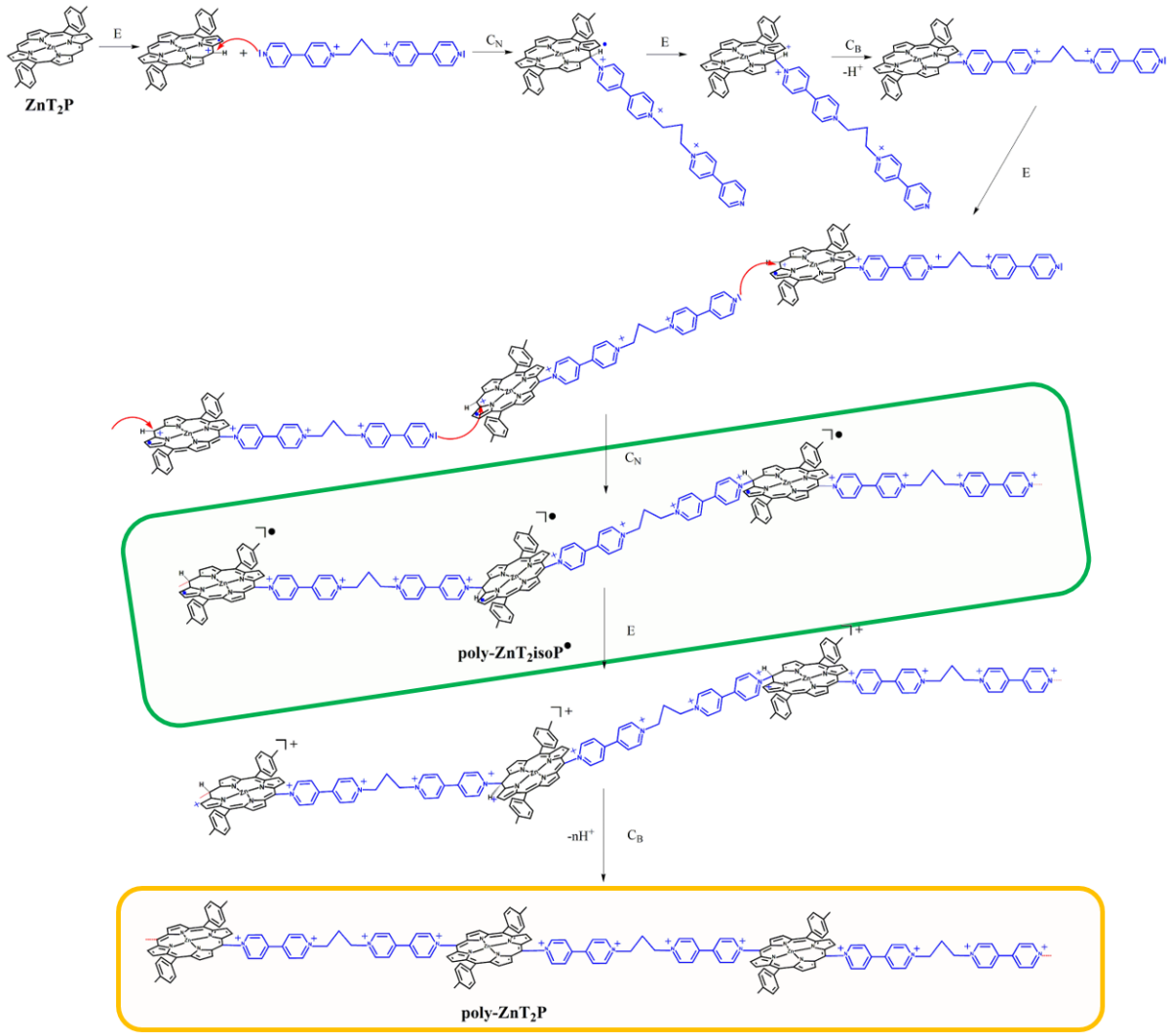

Scheme 2. Proposed plausible $(E_1C_{Nmeso}E_2C_B)_n$ mechanism of the formation of the intermediate **poly-ZnT$_2$isoP$^\bullet$** (green box) and the final **poly-ZnT$_2$P** (yellow box) copolymer explaining the reactivity of a $bpy^+–(CH_2)_3–^+bpy\cdot 2PF_6^-$ during the oxidation of **ZnT$_2$P. Poly-ZnT$_2$isoP$^\bullet$** is obtained using iterative scan between -1.0 V and 1.0 V and **poly-ZnT$_2$P** is obtained in the case of iterative scan between -1.0 V and 1.6 V.

During the electropolymerization of **ZnT$_2$P** in the presence of $bpy^+–(CH_2)_3–^+bpy\cdot 2PF_6^-$, when the anodic potential limit is 1.60 V, we observed that the oxidation peaks intensity increases (Fig. 2A) which is correlated to the increase of the film thickness. The first scan toward negative potentials reveals only one irreversible pyridinium-centered reduction. Starting with the second scan, in the cathodic potential range, the reduction peaks observed at ca. -0.13 V (peak I) and -0.63 V (peak II) *vs.* SCE for **poly-ZnT$_2$P** (Fig. 2A) have been attributed to electron transfers on the electrogenerated viologen units introduced between two porphyrins [52,57-58,60]. Peak a is attributed to the reduction of an oxidized isoporphyrin intermediate as previously described [5,29].

The continuous increase of these reduction waves indicates a regular growth of the copolymer film onto the ITO working electrode.

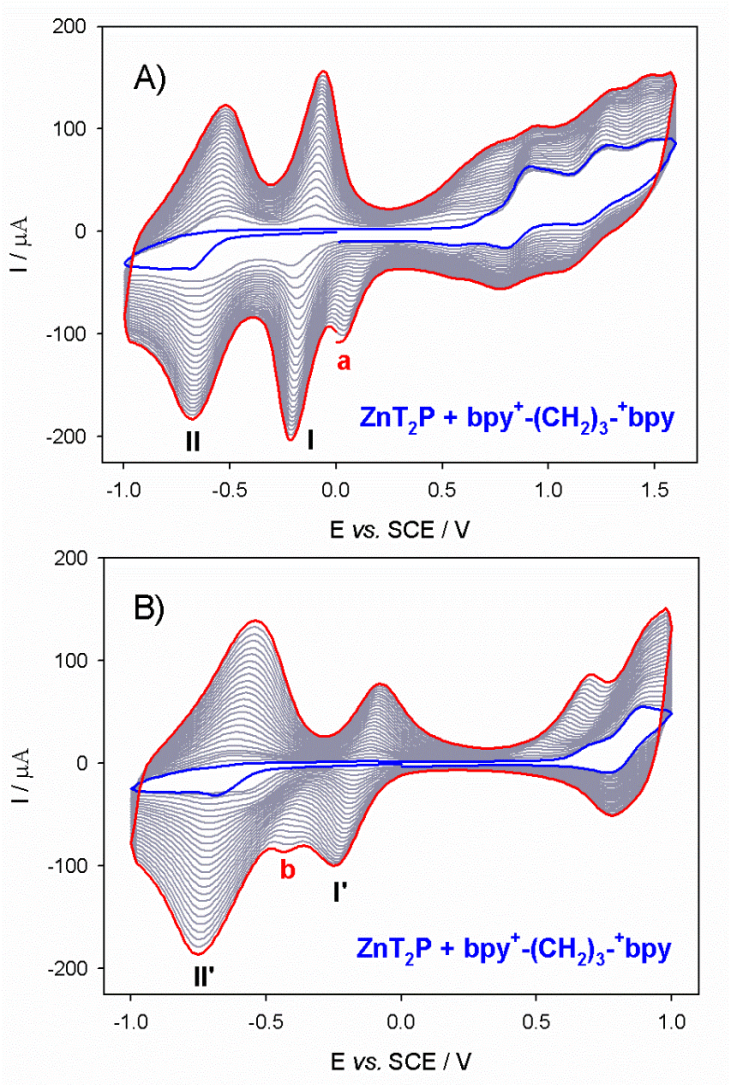

Fig. 2. Cyclic voltammograms recorded during 25 iterative scans conducted between A) -1.00 V and +1.00 V/SCE and B) -1.00 V and +1.60 V *vs.* SCE in a 1,2-$C_2H_4Cl_2$/CH_3CN (7/3) solution of **ZnT$_2$P** (0.25 mmol L^{-1}) in the presence of $bpy^+–(CH_2)_3–^+bpy·2PF_6^-$ (0.25 mmol L^{-1}) and NBu_4PF_6 (0.1 mol L^{-1}). WE: ITO. S = 1 cm^2. ν = 0.1 V s^{-1}. (a) This peak is attributed to the reduction of an oxidized isoporphyrin intermediate obtained if using 1.6 V as end potential during iterative scan. (b) This peak is attributed to the one electron reduction of the pyridium directly connected with the isoporphyrin. Peaks I': first reduction of the viologen (one electron reduction). Peak II': second reduction of the viologen (two electron reductions). Peaks I and II: successive reduction of the double viologen spacers. Blue curve: first scan (n=1). Red curve: final scan (n = 25). (For interpretation of the references to color in this figure legend, the reader is referred to the Web version of this article.)

During the electropolymerization of **ZnT$_2$P** in the presence of $bpy^+–(CH_2)_3–^+bpy·2PF_6^-$, when the anodic potential limit is +1.00 V (Fig. 2B), below the first porphyrin-based oxidation potential, the π-

radical cation **$ZnT_2P^{+\bullet}$** is produced. As a consequence, we observed significant changes during the electropolymerization process (Fig. 2B). In the anodic part, the intensity of the oxidation peak near +0.79 V corresponding to the first oxidation of **ZnT_2P**, continuously increases with no shift during the electropolymerization proving the formation of a new copolymer **poly-$ZnT_2isoP^{\bullet}$** in this potential range.

In the cathodic range, three successive reductions are observed at -0.18 V (peak I'), -0.44 V (peak b) and -0.70 V (peak II') (Fig. 2B). It must be noted that peak b is irreversible and peak I' is approximately half of the intensity than peak II'. These results point out to the formation of a copolymer **poly-$ZnT_2isoP^{\bullet}$** with different behavior than **poly-ZnT_2P**. We present below a detailed characterization of the two copolymers, i.e. **poly-ZnT_2P** and **poly-$ZnT_2isoP^{\bullet}$**. A comparison between their different properties is made when appropriate.

3.2. Electrochemical Quartz Crystal Microbalance (EQCM) for copolymers deposition

The electrosynthesis of **poly-$ZnT_2isoP^{\bullet}$** by electropolymerization with iterative scans between -1.00 and +1.00 V of (Fig. 3) has been monitored *in-situ* by EQCM. The variation of the quartz resonance frequency (Δf) decreases when the number of potential cycle increases, which is related to the increase of the amount of polymer deposited (Δm), calculated using Sauerbrey's equation [80].

Besides, the trace of the first scan in Fig. 3B shows a significant decrease of the resonance frequency and thus an increase of the deposited mass at the first oxidation of the porphyrin; i.e. electropolymerization occurs upon the formation of the radical cation porphyrin **$ZnT_2P^{+\bullet}$** in the presence of $bpy^{+}–(CH_2)_3–^{+}bpy\cdot 2PF_6^{-}$. The mass of the copolymer film increases with the number of potential cycle n (Fig. 3B). Note that a change of slope can be observed for n > 10 which might be related to a transition in the 3D architecture of the copolymer film and the incorporation of supporting electrolyte as well as solvent molecules.

After 25 iterative scans, 28.01 $\mu g/cm^2$ of **poly-$ZnT_2isoP^{\bullet}$** are deposited. The calculated surface coverage Γ in mole of repeat unit ($ZnT_2P\text{-}bpy^{2+}–(CH_2)_3–^{2+}bpy\cdot 4PF_6^{-}$) for the polymer is 18.8×10^{-9} $mol.cm^{-2}$. Similar behavior was observed for the electropolymerization of **poly-ZnT_2P** using iterative scans between -1.00 and +1.60 V (Fig. S4). Coverages after 25 iterative scans were about 35.38 $\mu g/cm^2$. The calculated surface coverage Γ in mole of repeat unit was 23.76×10^{-9} $mol.cm^{-2}$, a similar value to the one obtained for **poly-$ZnT_2isoP^{\bullet}$**.

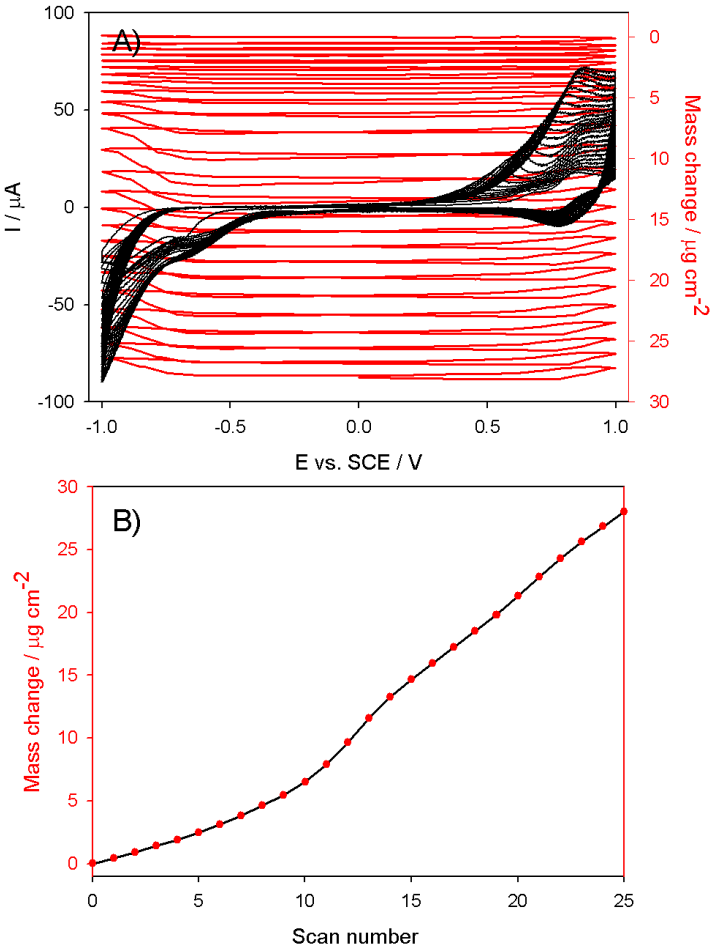

Fig. 3. A) Consecutive cyclic voltammograms (first 25 scans) between -1.0 V and +1.0 V and electrochemical quartz crystal microbalance measurements (Δm) for the first 10 scans during the formation of **poly-ZnT$_2$isoP$^\bullet$** obtained by the electropolymerization of 0.25 mmol L^{-1} **ZnT$_2$P** with 0.25 mmol L^{-1} bpy$^+$–(CH$_2$)$_3$–$^+$bpy·2PF$_6^-$ (0.25 mmol L^{-1}) in 1,2-C$_2$H$_4$Cl$_2$–CH$_3$CN (7/3) in the presence of 0.1 mol L^{-1} NBu$_4$PF$_6$. Working electrode: ITO (A = 0.2 cm^2) deposited on a 9.08 MHz AT-cut quartz crystal. v = 100 mVs^{-1}. B) Mass change (Δm) of the first 25 scans calculated from Sauerbrey's equation *versus* the number of scan n.

3.3. UV–Vis-NIR spectroscopy

UV-visible-NIR spectra on ITO electrodes coated with the copolymer **poly-ZnT$_2$isoP$^\bullet$** and **poly-ZnT$_2$P** have been measured at various thickness and compared (Fig. 4 and Fig. S5 respectively). The absorption intensity of the chromophores increases linearly with iterative scan number (Fig. 4B).

These results have been confirmed by AFM experiments (Figs. 10-11 for **poly-ZnT$_2$isoP$^\bullet$**) where the thickness was found to increase also linearly *versus* the number of iterative scans.

A typical UV-visible-NIR spectrum of **poly-ZnT$_2$isoP$^\bullet$** obtained after electropolymerization between -1.00 and +1.00 V exhibited a broad split Soret absorption band at λ = 432 nm and λ = 473 nm. The bands were red-shifted by 17 and 58 nm respectively compared to the **ZnT$_2$P** monomer (Table 2 and

Fig. 4). The visible bands (Q bands), observed at 571 and 635 nm, are also red-shifted by 25 and 51 nm compared to **ZnT$_2$P** and an additional band at 831 nm in the NIR region is also detected (Fig. 4A). These electropolymerized films have been found to be fully soluble in DMF. Analysis of **poly-ZnT$_2$isoP$^\bullet$** in solution by UV-Vis-NIR absorption spectroscopy revealed comparable spectra than the ones recorded on the solid film (Fig. 5).

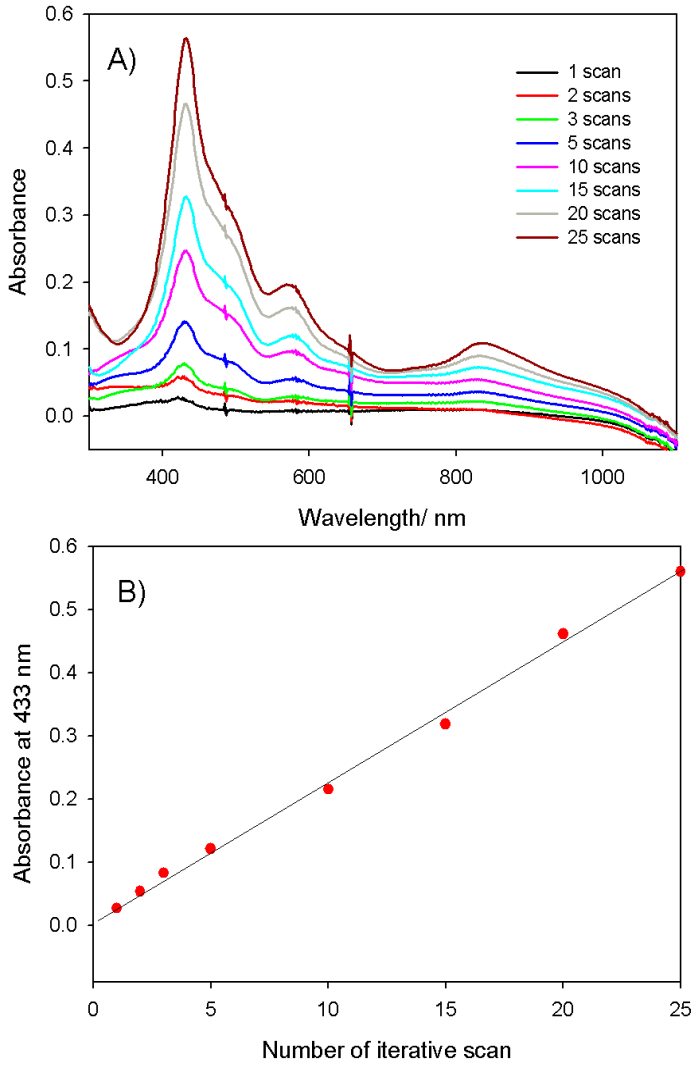

Fig. 4. A) UV-visible-NIR absorption spectra of **poly-ZnT$_2$isoP$^\bullet$** onto ITO with different numbers of iterative scans between -1.00 and +1.00 V *vs.* SCE (v = 100 mVs^{-1}). Only one side is covered by ITO. B) Plot of the absorbance measured at λ = 433 nm *versus* n the numbers of iterative scans. (For interpretation of the references to color in this figure legend, the reader is referred to the Web version of this article.)

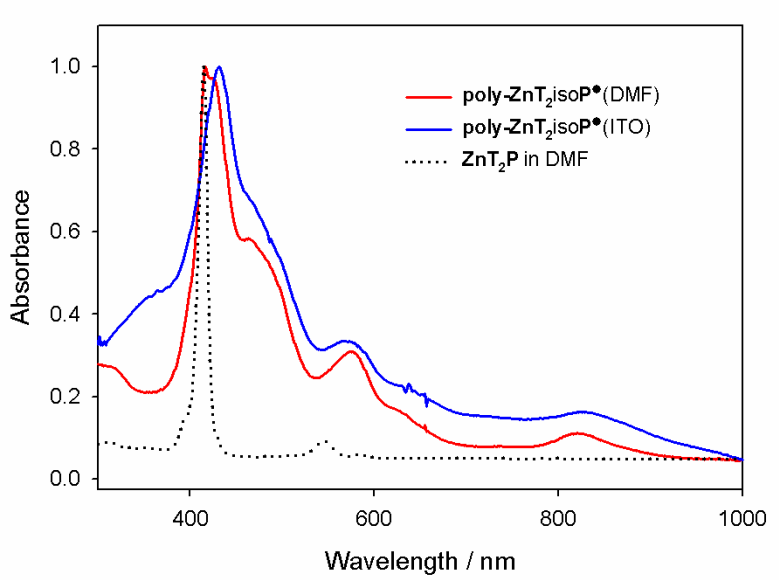

Fig. 5. Normalized UV-Vis-NIR spectra of the ITO electrode modified with **poly-ZnT2isoP•**, obtained with 10 iterative scans between -1.00 and +1.00 V *versus* SCE at v = 100 mVs^{-1} (blue line), and **poly-ZnT2isoP•** (red line) and **ZnT2P** (dark dotted line) in DMF solution. (For interpretation of the references to color in this figure legend, the reader is referred to the Web version of this article.)

The superposition of the UV-visible-NIR absorption spectra of **ZnT2P** in solution and of the copolymer **poly-ZnT2isoP•** deposited on ITO are compared in Figure 5. It reveals that the Soret band, attributed to the main porphyrin-based π-π* electronic transition, is much broader, split and more red-shifted for **poly-ZnT2isoP•** on ITO electrodes than for **ZnT2P** (Table 2).

The red shift of the Soret (B) and the Q bands might result from the presence of the electron-withdrawing pyridinium groups as well as from the nonplanar conformation of the macrocycle. Optical red shifts induced by the non-planarity of porphyrins are well documented [81-84] and have been rationalized by a larger destabilization of the highest occupied molecular orbitals (HOMOs) relative to the lowest unoccupied molecular orbitals (LUMOs) resulting in smaller HOMO to LUMO gaps [85-88]. These changes can also be understood taking into account the presence of intra- and intermolecular exciton-coupling between the porphyrin macrocycle within the copolymer [89-90].

The additional bands at 473 and 831 nm may be attributed to the isoporphyrin structure present in the copolymer. Similar bands have been already observed in the case of stable isoporphyrin monomer [16]. Interestingly, the broadening and the splitting of the Soret band as well as the presence of one additional band in the NIR between 750 nm and 1000 nm are expected to be advantageous to photovoltaic applications by extending the domain of solar light absorption.

Poly-ZnT$_2$isoP$^\bullet$ isoporphyrin radical film was found to be highly stable in the presence of oxygen (still stable even after one year). The isoporphyrin radical **Poly-ZnT$_2$isoP$^\bullet$** is also stable in DMF solution.

We have also investigated various copolymer **poly-ZnT$_2$P** (Fig. S5 and Scheme S1) coated films, prepared by changing the number of iterative scans n used for electropolymerization (between -1.00 V and +1.60 V). They exhibited only one large Soret absorption band at λ = 429 nm with a red shift of 14 nm compared to the **ZnT$_2$P** monomer (Table 2 and Fig. S5-S6). Again, a plot of the absorbance recorded at λ = 429 nm (Soret band of the porphyrin) as a function of the number of iterative scans n (Fig. S5) shows a quasi-linear increase of the intensity of the chromophore.

However, the additional band at 473 nm was nearly not detected. It suggested that at higher applied potential, isoporphyrin copolymer intermediate could be consumed giving the final structure of the copolymer with double viologen as spacers. But the consummation is not quantitative as seen in Figures S5-S6 probably due to *i*) the important thickness of the film and *ii*) to the difficulty to fully oxidized the film if using scan rate of 100 mVs^{-1}.

Table 2. UV–visible spectral data for **ZnT$_2$P**, and bpy$^+$–(CH$_2$)$_3$–$^+$bpy·2PF$_6^-$ in 1,2-EtCl$_2$, **poly-ZnT$_2$P$^\bullet$** and **poly-ZnT$_2$P** on optical transparent ITO electrodes. Under bracket: molar extinction coefficient (ε /10^3 L.M.cm^{-1}).

Compound	Soret band/nm	Q bands/nm	π-π^*Band/nm
ZnT$_2$P	415 (405.4)	546 (18.9), 584 (4.9)	
ZnT$_2$P-bpy$^+$SbCl$_6^-$ [a]	429 (584.8)	561 (42.4), 611 (18.1)	
bpy$^+$–(CH$_2$)$_3$–bpy$^+$ 2PF$_6^-$ [a]			266 (40.8)
poly-ZnT$_2$isoP$^\bullet$ [b]	432, 473 (shoulder)	571, 635, 831	
poly-ZnT$_2$isoP$^\bullet$ [c]	415,[f] 423 (shoulder), 463 (shoulder)	573, 631, 825	
poly-ZnT$_2$P[d]	429	573, 614, 811	
poly-ZnT$_2$P[e]	415,[f] 429	573, 614 ,811	

[a] In CH$_3$Cl.
[b] Copolymers obtained by iterative scan between -1.00 V and +1.00 V *vs.* SCE onto ITO.
[c] Copolymers obtained by iterative scan between -1.00 V and +1.00 V *vs.* SCE in DMF.
[d] Copolymers obtained by iterative scan between -1.00 V and +1.60 V *vs.* SCE onto ITO.
[e] Copolymers obtained by iterative scan between -1.00 V and +1.60 V *vs.* SCE in DMF.
[f] Soret band of the **ZnT$_2$P** monomer which was encapsulated in the film during the electropolymerization and liberated during dissolution of **poly-ZnT$_2$isoP$^\bullet$**.

3.4. Cyclic voltammetric investigations of the copolymeric films.

3.4.1. Cyclic voltammetric investigations of the poly-$ZnT_2isoP^{\bullet}$ film.

Electroactive polymers deposited by cyclic voltammetry (n iterative scans) on ITO surfaces have been characterized by electrochemical methods. The CV curves shown in Figure 6 have been recorded with a copolymer grown on the electrode surface for various potential scans (n = 2, 3, 5, 10, 15, 20 cycles) between -1.0 V and +1.0 V. The electrode was then removed from the electrochemical cell, washed with CH_3CN and used as working electrode in a clean electrolytic solution containing only the solvent and the supporting electrolyte.

Three successive waves are observed for **poly-$ZnT_2isoP^{\bullet}$** during the cathodic scan (Table 3 and Fig. 6AB), the first and the last being reversible. The first well defined, bell-shaped, reduction wave observed at –0.18 V vs. SCE (peak I') is attributed to the formation of viologen radical cations in the copolymer (-ZnT_2isoP-$^{\bullet}$py-py^{+}–$(CH_2)_3$–$^{+}$py-py^{+}-ZnT_2isoP-). The second wave (peak a) detected at -0.62 V is irreversible and very close to the last process (peak II'). This wave (peak b) corresponds probably to the reduction of the pyridinium connected to the isoporphyrin (ZnT_2isoP-$^{\bullet}$py-py^{+}–$(CH_2)_3$–$^{+}$py-py$^{\bullet}$-ZnT_2isoP-) while the last wave reversible well defined, bell-shaped, reduction wave observed (peak II') is attributed to the second viologen-centered electron transfer (two-electron transfer *per* spacer giving ZnT_2isoP-py-py–$(CH_2)_3$–py-py-ZnT_2isoP-). The reduction of the monomer py-py^{+}–$(CH_2)_3$–$^{+}$py-py 2 PF_6^{-} is measured at -0.68 V.

Additionally, **poly-$ZnT_2isoP^{\bullet}$** films electropolymerized between by -1.0 V and 1.0 V, can be further oxidized up to 1.6 V (Fig. 7). Oxidation of the isoporphyrin radical units which give oxidized isoporphyrin is then possible. At this stage, the hydrogen atom located on the *meso*-carbon can be released giving copolymer with similar redox properties than **poly-ZnT_2P**. Thus, it is feasible to oxidize the radical isoporphyrin **poly-$ZnT_2isoP^{\bullet}$** copolymer and then remove the hydrogen atom located on the *meso*-carbon giving the formation of **poly-ZnT_2P** with a double viologen spacer (Scheme 3).

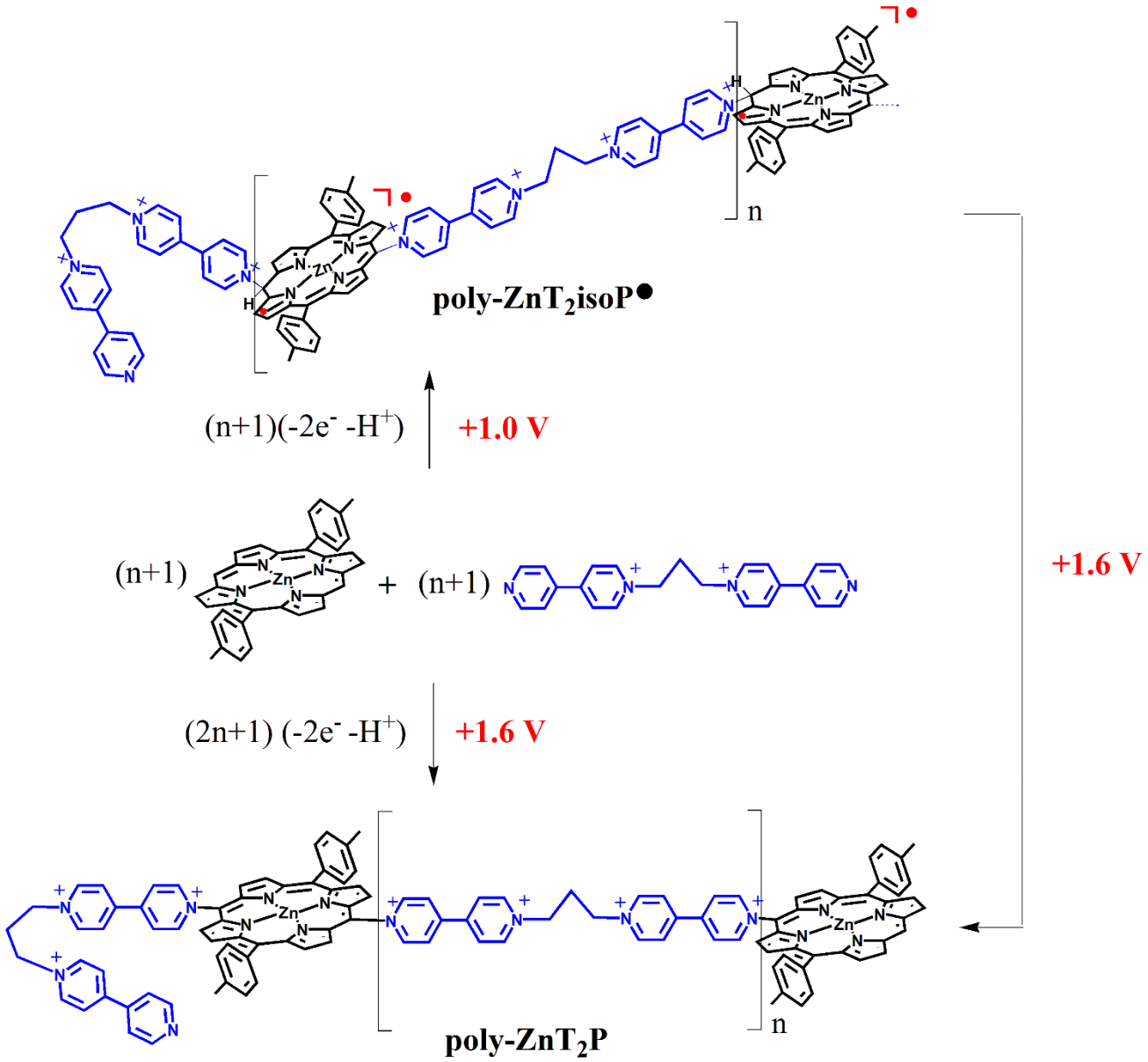

Scheme 3. Electropolymerization scheme explaining the reactivity of $bpy^{+}–(CH_2)_3–^{+}bpy\cdot 2PF_6^{-}$ in the presence of **ZnT₂P** in the case of iterative scan between -1.0 V and 1.0 V or between -1.0 V and 1.6 V.

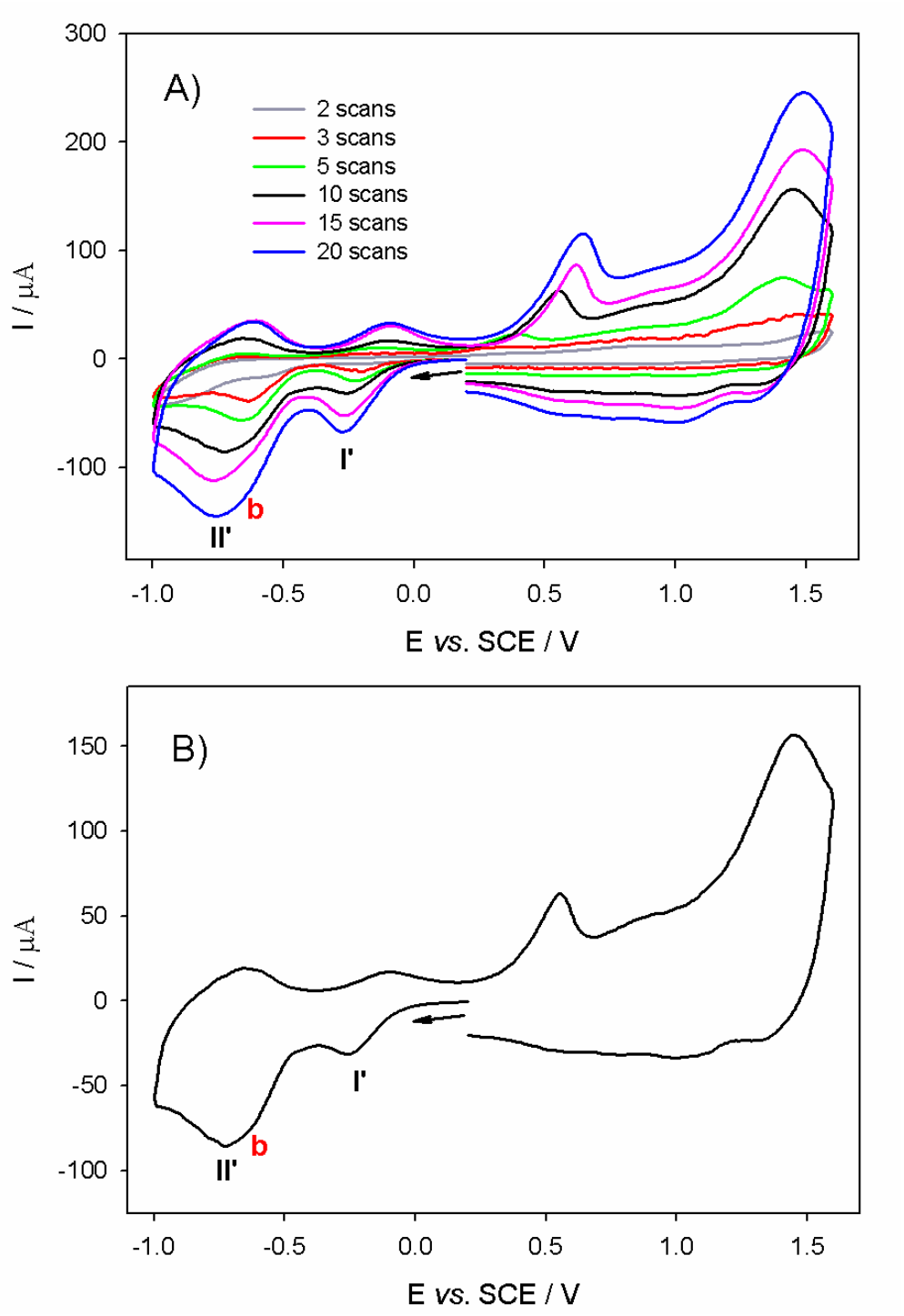

Fig. 6. Cyclic voltammograms of **poly-ZnT$_2$isoP$^\bullet$** obtained with bpy$^+$–(CH$_2$)$_3$–$^+$bpy·2PF$_6^-$ and **ZnT$_2$P** after A) n = 2, 3, 5, 10, 15 and 20 scans and B) after 10 scans between -1.0 V and +1.0 V in CH$_3$CN/1,2-C$_2$H$_4$Cl$_2$ (3/7) with 0.1 M NBu$_4$PF$_6$. WE: ITO. S = 1 cm^2, v = 0.1 V s^{-1}. Irreversible peaks not labelled in anodic part correspond to the oxidation of the π-ring of the macrocycle.

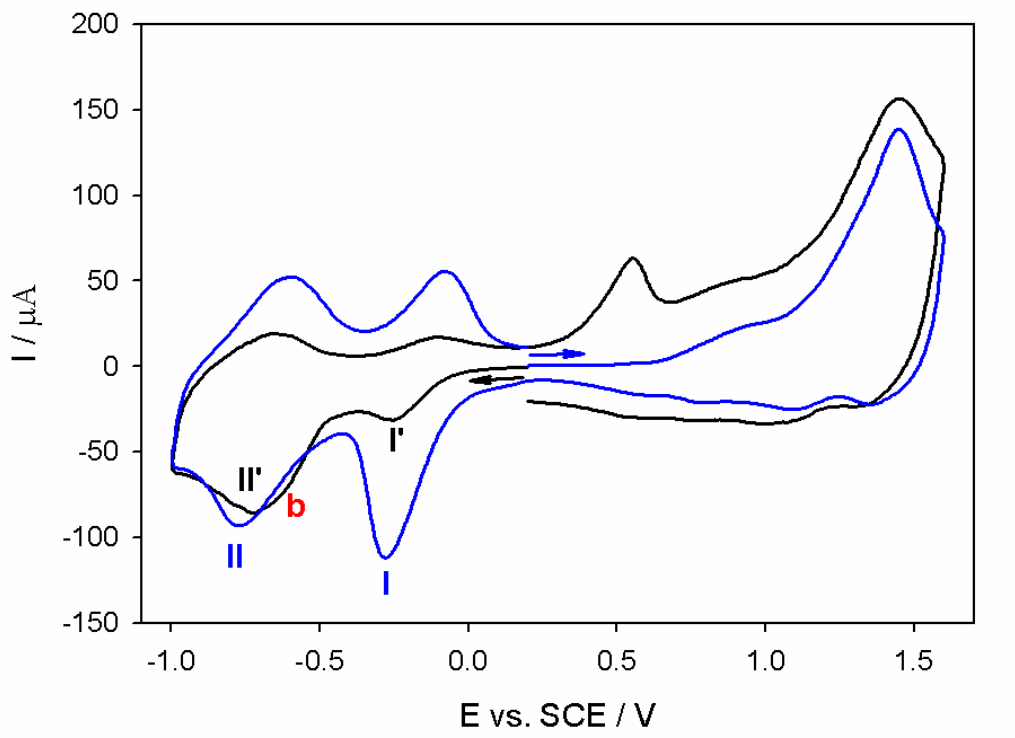

Fig. 7. Cyclic voltammograms of **poly-ZnT$_2$isoP$^{\bullet}$** obtained with bpy^{+}–(CH$_2$)$_3$–$^{+}$bpy·2PF$_6^-$ and **ZnT$_2$P** after n = 10 scans, using iterative scan between -1.0 V and +1.0 V in CH$_3$CN/1,2-C$_2$H$_4$Cl$_2$ (3/7) with 0.1 M TBAPF$_6$. WE: ITO. S = 1 cm^2. *v* = 0.1 V s^{-1}. Blue curve: the direction of the potential scan is reversed (in comparison to the black curve) using new electrode. Global reaction of the conversion of **poly-ZnT$_2$isoP$^{\bullet}$** to **poly-ZnT$_2$P** during oxidation at 1.60 V (blue curve) is described in Scheme 3. Peaks I and II correspond to the formation of the bis-radical cation viologen (couple V^{2+}–(CH$_2$)$_3$–V^{2+}/V$^{+\bullet}$–(CH$_2$)$_3$–V$^{+\bullet}$, peak I) and the second reduction of two bis-radical cation viologen units of the spacers yielding V^0–(CH$_2$)$_3$–V^0 (couple V$^{+\bullet}$–(CH$_2$)$_3$–V$^{+\bullet}$/ V^0–(CH$_2$)$_3$–V^0, peak II). V = py-py. (For interpretation of the references to color in this figure legend, the reader is referred to the Web version of this article.)

Table 3. Electrochemical data for **ZnOEP**, **ZnT$_2$P**, **bpy$^+$–(CH$_2$)$_3$–$^+$bpy 2PF$_6^-$**, **poly-ZnT$_2$P**, and **poly-ZnT$_2$isoP$^\bullet$**.

Compounds	Ring oxidation		Reduction of spacer			Ring reduction	
			peak I or I'	bpy$^+$/bpy$^\bullet$ or **peak b**	peak II or II'		
ZnOEP[a]	1.08 (130)	0.71 (128)				-1.66	
ZnT$_2$P[a]	1.08 (150)	0.79 (90)				-1.41 (160)	-1.84 (170)
bpy$^+$–(CH$_2$)$_3$–$^+$bpy·2PF$_6^-$				-0.68^{irr}			
poly-ZnT$_2$isoP$^\bullet$	+1.45^{irr}	+0.89^{irr}	-0.18 (140)	**-0.62^{irr}**	-0.70 (70)		
poly-ZnT$_2$P	+1.35^{irr}	+1.09 (130)	-0.13 (170)		-0.63 (120)		

[a] Potentials in V *vs.* SCE were obtained from cyclic voltammetry in 1,2-C$_2$H$_4$Cl$_2$ with 0.1 mol L^{-1}TBAPF$_6$. Scan rate = 100 mV s^{-1}. Working electrode: ITO, S=1 cm^2.
[b] Potentials in V *vs.* SCE were obtained from cyclic voltammetry in CH$_3$CN/1,2-C$_2$H$_4$Cl$_2$ (3/7) with 0.1 mol L^{-1} TBAPF$_6$. Scan rate = 100 mV s^{-1}.
[c] Potentials in V *vs.* SCE were obtained from cyclic voltammetry in H$_2$O with 0.5 mol L^{-1} NaI. Working electrode: glassy carbon electrode. Scan rate = 100 mV s^{-1} (see Fig. S15).
The given half-wave potentials are equal to $E_{1/2} = (E_{pa} + E_{pc})/2$. Under bracket: $\triangle E_p = |E_{pa} - E_{pc}|$.

3.4.2. Cyclic voltammetric investigations of the poly-ZnT$_2$P film.

Electropolymerization using iterative scan between -1.00 V and 1.60 V *vs.* SCE in the presence of **ZnT$_2$P** and bpy$^+$–(CH$_2$)$_3$–$^+$bpy·2PF$_6^-$, was also performed to obtain **poly-ZnT$_2$P** film with double viologen spacers (Scheme 2). **Poly-ZnT$_2$P** copolymers were studied in the electrolyte used for electropolymerization that is CH$_3$CN/1,2-C$_2$H$_4$Cl$_2$ (3/7) solution with 0.1 M NBu$_4$PF$_6$.

In contrast with **poly-ZnT$_2$isoP$^\bullet$**, no irreversible wave was detected in the cathodic part and only two successive reversible reductions (peaks I and II) were measured.

The two reduction peaks centered at ca. -0.13 V (peak I) and -0.63 V (peak II) correspond to the formation of the bis-radical cation viologen (couple V^{2+}–(CH$_2$)$_3$–V^{2+}/V$^{+\bullet}$–(CH$_2$)$_3$–V$^{+\bullet}$, V = py-py,

peak I) and the second reduction of two bis-radical cation viologen units of the spacers yielding V^0-$(CH_2)_3$-V^0 (couple $V^{+\bullet}$–$(CH_2)_3$–$V^{+\bullet}$/ V^0–$(CH_2)_3$–V^0, peak II) (Table 3, Fig. 8 and Fig. S6).

It must be noted that under the measurement conditions, the splitting of the second reduction wave of the viologen, observed with the **ZnOEP** porphyrin [52] was not detected in the case of **ZnT$_2$P** porphyrin.

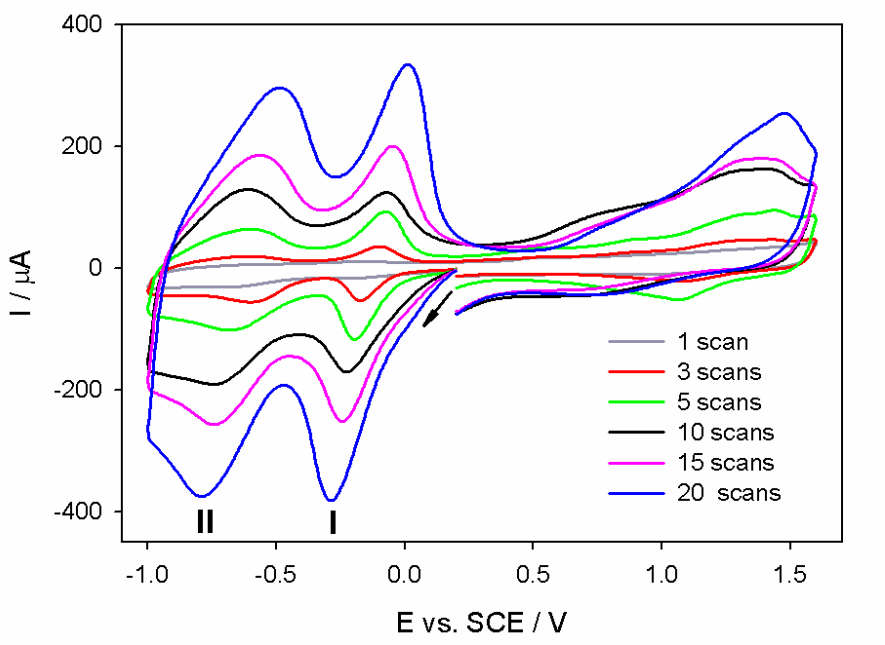

Fig. 8. A) Cyclic voltammograms of **poly-ZnT$_2$P** obtained with bpy^+–$(CH_2)_3$–$^+$bpy·$2PF_6^-$ and **ZnT$_2$P** after n = 1, 2, 3, 5, 10, 15 and 20 scans, between -1.0 V and +1.6 V in CH_3CN/1,2-$C_2H_4Cl_2$ (3/7) with 0.1 M NBu_4PF_6. WE: ITO. S = 1 cm^2. *v* = 0.1 V s^{-1}. (For interpretation of the references to color in this figure legend, the reader is referred to the Web version of this article.)

3.5. Electron spin resonance (ESR) spectroscopy

Copolymer **poly-ZnT$_2$PisoP•** onto ITO glass prepared after 50 iterative scans was inserted directly to the ESR cavity and the spectrum (Fig. S7 in ESI) recorded at room temperature shows spectral contributions from two paramagnetic species. The dominant feature shows a broad signal of six lines and comes from an impurity in the ITO glass. A less intense line is observed in the middle of the spectrum and probably arises from an organic radical.

To confirm the presence of the organic radical, **poly-ZnT$_2$isoP•** films onto ITO were prepared with the same conditions (25 iterative scans between -1.0 V and 1.0 V, v = 100 $mV.s^{-1}$).

Poly-ZnT$_2$isoP• was then removed from ITO using DMF. The operation was repeated three times. The obtained solutions were degassed and transferred to a capillary. The ESR spectrum shown in

Figure 9 reveals probably the presence of the radical centered on the isoporphyrin (g=2.0026, linewidth=6 G) [91]. Increasing the concentration of the deposited copolymer on the ITO glass leads to an enhancement of the ESR intensity (Fig. S8 in ESI).

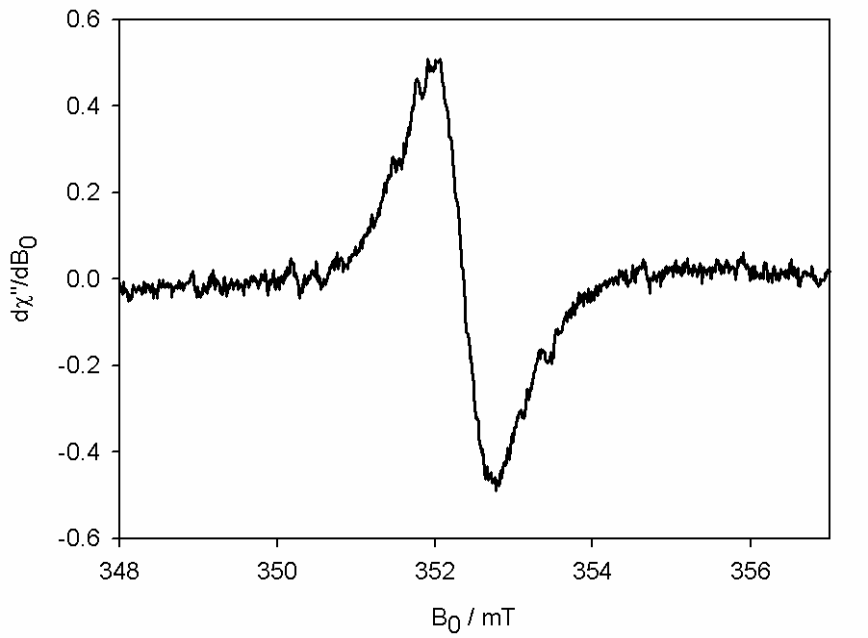

Fig. 9. X-Band EPR spectrum in DMF of **poly-ZnT$_2$isoP$^\bullet$** at room temperature. The solution of **poly-ZnT$_2$isoP$^\bullet$** was prepared by washing with 160 μL of DMF the covered ITO obtained using 25 scans between -1.0 V and 1.0 V, v = 100 mV.s^{-1}. In order to have enough solution, the operation was repeated three times.

Usually, isoporphyrin or radical cations porphyrins are reactive and undergo facile degradation. In this study, **poly-ZnT$_2$isoP$^\bullet$** isoporphyrin radical film is remarkably stable for one year at the solid state (in air). This stability may be due to the *i*) electron-withdrawing groups which significantly facilitate the reduction and stabilize the radical cation, *ii*) the delocalization of the radical through the porphyrin as well as intermolecular π–π -stacking and π-dimerization between macrocycles.

3.6. Film Morphology (Atomic Force Microscopy)

3.6.1. Film Morphology (Atomic Force Microscopy) of poly-ZnT$_2$isoP$^\bullet$ copolymer.

The films obtained by iterative scan between -1.0 V and +1.0 V were studied by scanning atomic force microscopy (AFM) (Figs. 10-11, Figs. S9-S10). In a characteristic picture for **poly-ZnT$_2$isoP$^\bullet$**, copolymer appears on the surface as tightly packed coils with an average diameter of ca. 60-70 nm, the height being around 8.0 nm for the film obtained after 3 iterative scans between -1.0 V and +1.0 V (Fig. 10). The rms surface roughnesses of the two films have been estimated at 2.0 nm for **poly-ZnT$_2$isoP$^\bullet$**, (calculated from an area of 1.0 μm^2 in Figure 10). The **poly-ZnT$_2$isoP$^\bullet$** copolymer

obtained after higher iterative scan number exhibited comparable morphology but showed in several positions some aggregation of the coils accompanied by a larger value of the rms surface roughness (8.8 nm for n = 10). The formation of coil aggregates might be related to the change of slope of the deposited mass, observed from EQCM measurements in Figure 3.

The **poly-ZnT$_2$P** films were also studied by AFM (Fig. S11). The **poly-ZnT$_2$P** copolymer appears on the surface yet again as tightly packed coils with an average diameter of ca. 120-150 nm, the height being around 25-30.0 nm for the film obtained after 20 iterative scans (n = 20). The rms surface roughness of the films has been estimated at 3.0 nm.

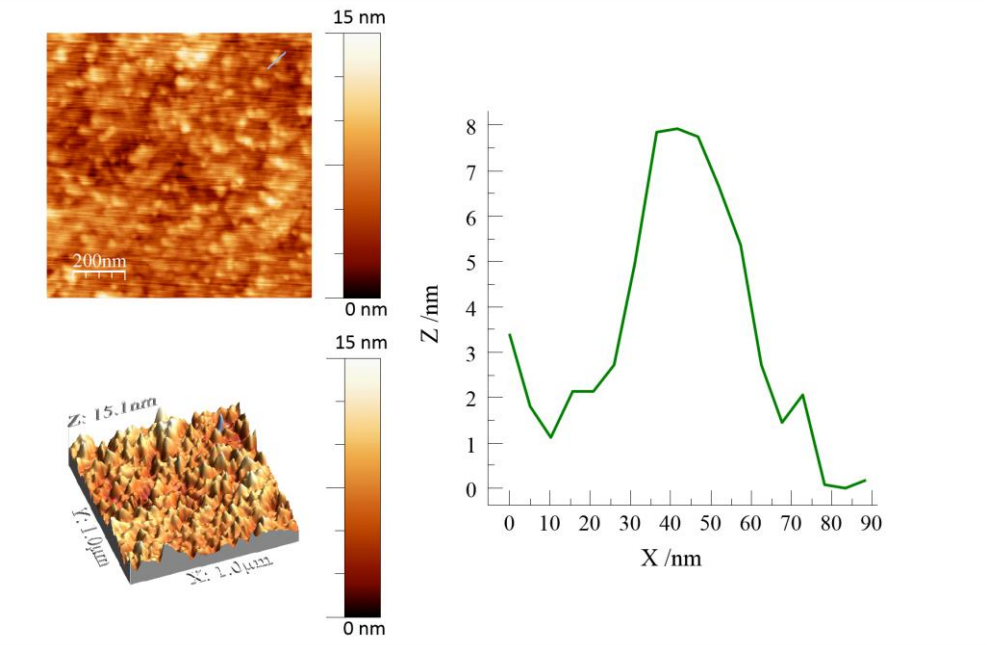

Fig. 10. Left: Tapping mode AFM topography of **poly-ZnT$_2$isoP$^\bullet$** (deposition between -1.0 V and +1.0 V vs. SCE on ITO, n = 3). Right: section analysis of the aggregate marked by a blue line. (For interpretation of the references to color in this figure legend, the reader is referred to the Web version of this article.)

3.6.2. Thickness measurement of copolymeric films

The thicknesses of the **poly-ZnT$_2$isoP$^\bullet$** copolymer (Fig. 11) have been estimated upon scratching the film with a metallic tip and measuring the relative heights on each side of the scratch (Fig. 11AB). The thickness measured by AFM was found to increase with the deposition time to reach an upper limit value for all the films studied. This trend is in line with the data recorded by UV-Vis-NIR absorption spectroscopy. The thickness measured after ten iterative scans (scan rate 100 mVs^{-1}) was estimated to 30 nm for **poly-ZnT$_2$isoP$^\bullet$** (Fig. 11CD, dark cyan triangle up).

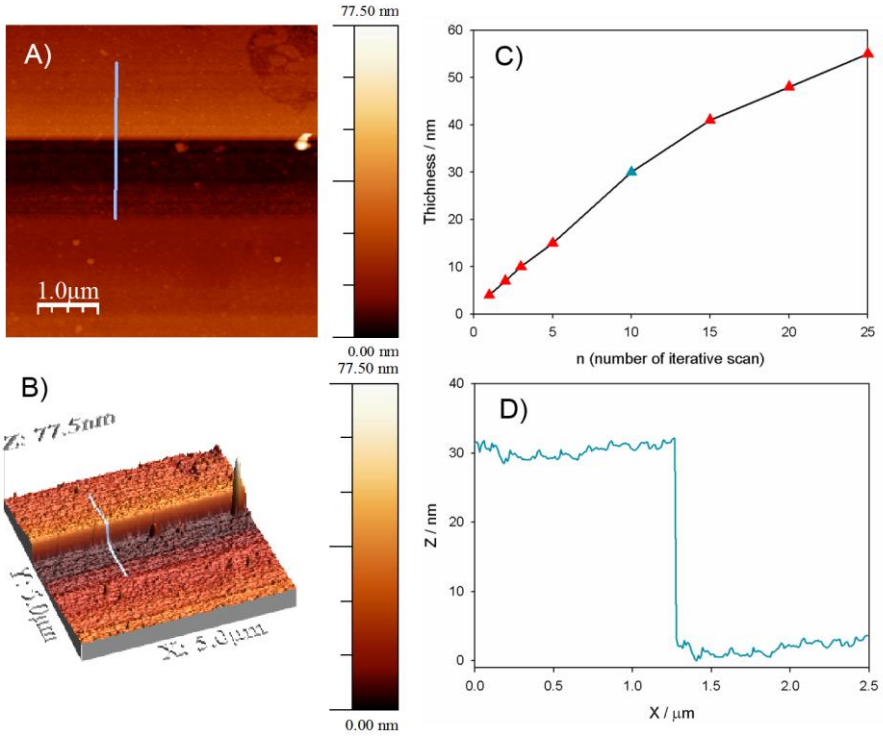

Fig. 11. A) Tapping mode AFM topography (AFM, surface plot, 2D top view) image of the modified ITO electrode with **poly-ZnT$_2$isoP$^{\bullet}$** obtained after 10 iterative scans. B) AFM 3D image and section analysis. C) Thickness measured from AFM *versus* different numbers of iterative scans (between -1.0 and 1.0 V *vs.* SCE). The dark cyan triangle up corresponds to the measurement obtained from B) and D). D) Section analysis. (For interpretation of the references to color in this figure legend, the reader is referred to the Web version of this article.)

3.7. X-ray photoelectron spectra (XPS) of copolymers

The copolymer films were also investigated by X-Ray photoelectron spectroscopy. The analysis of the survey spectra of **poly-ZnT$_2$isoP$^{\bullet}$** (Fig. S12) confirms the presence of the isoporphyrin and of the and the $-V^{2+}-(CH_2)_3-V^{2+}-$ spacer (Zn 2p3 at 1021.7 eV, N 1s, and C 1s peaks), while the signals for F 1s (686.6 eV), and P 2p (136.7 eV) electrons stem from the incorporated counterion PF_6^- to equilibrate the pyridiniums charges. The C1s peaks are composed of two signals at 284.8 and 286.5 eV attributed to homo and hetero (connected to nitrogen) carbon atoms respectively. The N1s peaks reveal the presence of three chemically different nitrogens. The contributions at 398.6 eV and 400.3 eV are attributed to the iminic nitrogen and to the reduced bispyridinium respectively. The peaks at ca. 402.3 eV might result from the viologen groups and the presence of tetrabutylammonium in the film. The O 1s signal comes from H_2O adsorbed on the copolymer surface [92]. Similar behavior is observed for **poly-ZnT$_2$P** film (Fig. S13)

3.8. Photoelectrochemical properties

Figure 12A shows the typical current-potential curves of **poly-ZnT$_2$isoP$^\bullet$** and **poly-ZnT$_2$P** thin films on ITO electrodes obtained in 5 mM I_2 / 0.5 M I^- aqueous solution.

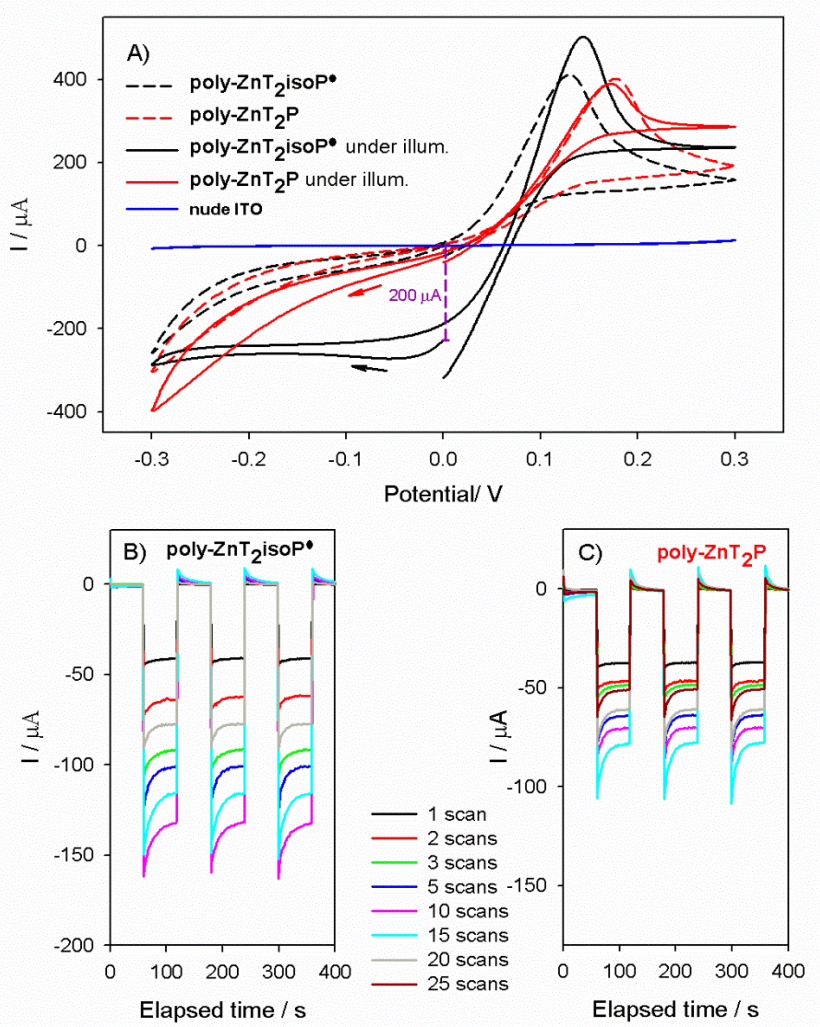

Fig. 12. A) Current-potential curves of **poly-ZnT$_2$isoP$^\bullet$** (obtained with n = 10 iterative scans between -1.0 V and +1.0 V) and **poly-ZnT$_2$P** (obtained with n = 10 iterative scans between -1.0 V and +1.6 V) thin films on ITO electrodes obtained in 0.5 M I^- / 5 mM I_2 aqueous solution in the dark or under visible illumination. B) and C) Photoelectrochemical response of **poly-ZnT$_2$isoP$^\bullet$** and **poly-ZnT$_2$P** films obtained with n = 1, 2, 3, 5, 10, 15, 20 or 25 iterative scans. Measurements has been done under on-off light illumination from a 300 W Xe arc lamp (with λ > 385 nm long pass filter) in I_3^- 5 mmol L^{-1} and I^- 0.5 mol L^{-1} aqueous solution. BIAS potential: 0.00 V *vs.* OCP. (For interpretation of the references to color in this figure legend, the reader is referred to the Web version of this article.)

The equilibrium potential of I_3^-/I^- redox couple in solution is taken as reference potential at 0 V in the cyclic voltammograms. For ten electropolymerization cycles, the amount of deposited copolymer on ITO substrate is approximately the same (ca. 6 µg/cm^2) for both **poly-ZnT$_2$isoP$^\bullet$** and **poly-ZnT$_2$P**

samples, thus enabling the comparison of their (photo)electrochemical properties. First, we analyze the curves obtained in the absence of illumination (plotted with dashed lines in Fig. 12A).

For bare ITO electrode (blue curve), almost no Faradaic current is observed between -0.3 and 0.3 V, revealing the slow I^- oxidation and I_3^- reduction kinetics on ITO. However, the I^- oxidation and I_3^- reduction currents are significantly enhanced on the ITO modified by the copolymers (black and red curves in Fig 12A).

For the I^- oxidation, anodic current peaks at ca. 0.1 V for **poly-ZnT$_2$isoP$^\bullet$** and at ca. 0.2 V for **poly-ZnT$_2$P** are observed. At this stage, the reasons why the I^- oxidation current goes through a maximum are unclear and further studies are required in order to explain this behavior.-Interestingly, the anodic peak potential is negatively shifted by ca. 0.1 V on **poly-ZnT$_2$isoP$^\bullet$** compared to **poly-ZnT$_2$P** suggesting that the I^- oxidation kinetics is significantly faster on the **poly-ZnT$_2$isoP$^\bullet$** modified electrode. In contrast, the I_3^- reduction current is slightly lower on **poly-ZnT$_2$isoP$^\bullet$** than on **poly-ZnT$_2$P** showing that the **poly-ZnT$_2$P** copolymer is a better catalyst for the I_3^- reduction than **poly-ZnT$_2$isoP$^\bullet$**.

The current-potential curves measured under visible light illumination and potentiodynamic conditions are also plotted in Figure 12A (full line) for the **poly-ZnT$_2$isoP$^\bullet$** and **poly-ZnT$_2$P** copolymers respectively. The photocurrent response in the potentiostatic mode at 0 V under on-off light illumination cycles is shown in Figure 12BC. Under visible light, the open circuit potential increases of ca. 80 and 30 mV for the **poly-ZnT$_2$isoP$^\bullet$** and **poly-ZnT$_2$P** copolymers respectively. Above this potential, the I^- oxidation current becomes predominant due to the high I^- concentration in solution, impeding thus further increase of the photovoltage. For potentials below the OCP, a negative photocurrent is observed for both copolymers, the photocurrent at 0 V of the **poly-ZnT$_2$isoP$^\bullet$** copolymer thin film reaching ca. -140 µA cm^{-2} (potentiostatic experiment) or -200 µA cm^{-2} (in the CV) while it is only ~~of~~ -70 µA cm^{-2} (potentiostatic experiment) or -30 µA cm^{-2} (in the CV) on **poly-ZnT$_2$P** for approximately the same amount of electrodeposited copolymer (see also Figs. S14-S15 in ESI).

The better performances of isoporphyrin copolymer can be tentatively attributed to the broad Soret absorption band improving the light harvesting efficiency in the visible range and then the photocurrent. It should be mentioned that the presence of an additional absorption band at 850 nm in the optical spectra of the isoporphyrin copolymer may also be beneficial for the photocurrent. For all the

copolymers, the photocurrent level remains stable after several hours of on-off illumination cycles at 0 V (not shown) indicating that the copolymers are stable under photocurrent generation.

Figure 13 represents the energy diagram corresponding to the photoreduction of I_3^- on the copolymer **poly-ZnT$_2$isoP$^\bullet$**. Energy diagram for **poly-ZnT$_2$P** is given in the ESI in Figure S20.

The HOMO level energies of the **poly-ZnT$_2$isoP$^\bullet$** and **poly-ZnT$_2$P** species have been estimated from the first oxidation potential observed in the CV, while the energy level of the dipyridinium species is given by the potential of the first reduction peak (Table 3). The LUMO levels of the excited **poly-ZnT$_2$isoP$^\bullet$** and **poly-ZnT$_2$P** species can be roughly estimated by subtracting the excitation energy of the Soret or Q bands from the HOMO level energies. The energy Level corresponding to the band in the NIR region has also been indicated in the energy diagram. Under illumination at 0 V, the photon absorption by the (iso)porphyrin entities generates an electron hole pair in the copolymer. The electron is transferred from the excited (iso)porphyrins to the I_3^- which is reduced into I^-, the double viologen spacer eventually acting as a relay for the electron transfer. The oxidized (iso)porphyrins are regenerated by an electron transfer from the ITO substrate. The I_3^- reduction is in competition with the recombination of the photogenerated electron-hole pair. Thus, fast electron transfer kinetics between the ITO and the oxidized (iso)porphyrins and/or between the excited (iso)porphyrins and the I_3^- are crucial for the efficient photocurrent generation. In principle, the photoelectrons may also be transferred from the excited (iso)porphyrins to the ITO electrode which would result in a positive I^- oxidation photocurrent. Such photoelectrochemical oxidation of I^- on electropolymerized porphyrin thin films was observed when I^- and I_3^- are in acetonitrile solution [52]. However, only negative photocurrents are observed when the copolymer is in aqueous solution suggesting that the photooxidation of I^- is not favoured in such case.

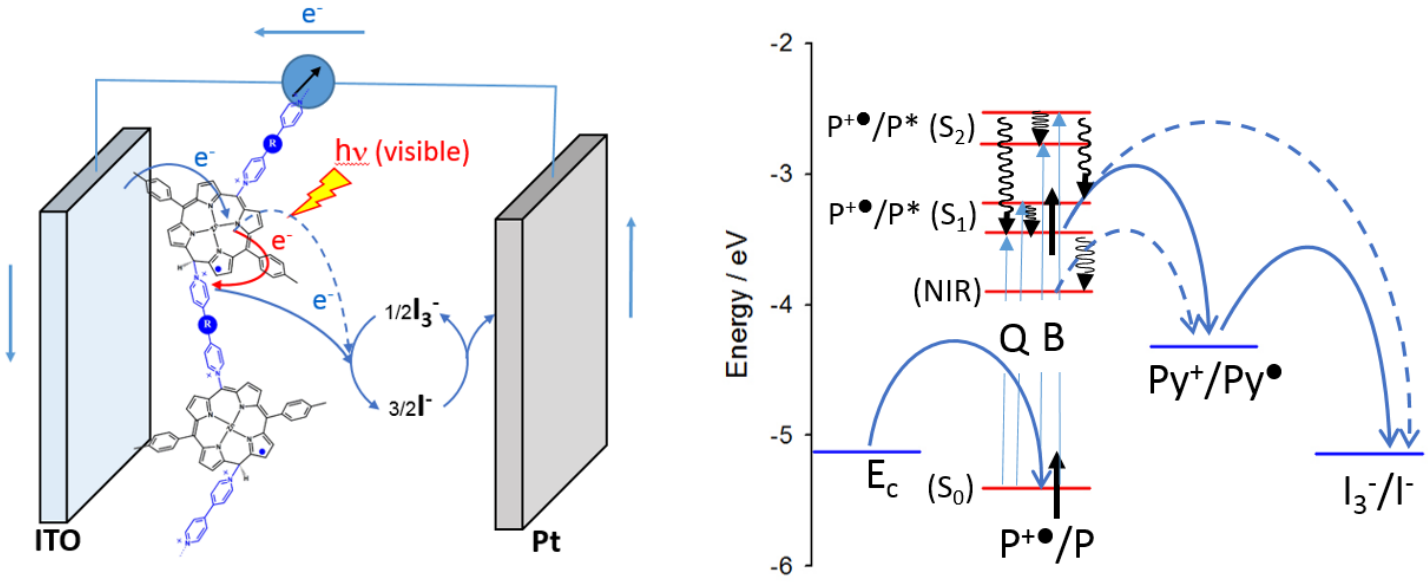

Fig. 13. Schematic illustration of the energy level diagram for **poly-ZnT$_2$isoP$^{\bullet}$** showing electron transfer processes in H_2O containing I_3^- 5 mmol L^{-1} and I^- 0.5 mol L^{-1} (Py^+ = pyridinium, P = porphyrin).

The magnitude of the photocurrent strongly depends on the number of potential scans n and then of the amount of copolymer film deposited as displayed in Fig. 12BC, Fig. 15A and Figs. S14-S15. For both copolymers, the photocurrent goes through an optimum as a function of n, the best performances being obtained for n=10 or 15 electropolymerization cycles. It is confirmed that higher photocurrents are obtained with the isoporphyrin copolymer **poly-ZnT$_2$isoP$^{\bullet}$** than **poly-ZnT$_2$P**.

Further insights into the photoelectrochemical behaviour of the copolymer films as a function of n could be gained by electrochemical impedance spectroscopy, which is widely used in the investigation of dye sensitized solar cell [93-95]. The Nyquist and Bode plots of a typical impedance spectra measured for (**poly-ZnT$_2$isoP$^{\bullet}$**) at 0 V in 5 mM I_3^- / 0.5 M I^- aqueous solution are plotted in Figure 14 for n=10. All the impedance spectra of the copolymer films (**poly-ZnT$_2$isoP$^{\bullet}$** and **poly-ZnT$_2$P)** obtained for various number of potential scans, n=1, 2, 3, 5, 10, 15 and 20 are given in supplementary information (Figs. S16-S19). For low n values (i.e. 1 or 2 scans), the Nyquist diagrams exhibit only one semi-circle, which can be modelled by the charge transfer resistance R_{ct} of the I^-/I_3^- species at the ITO/solution interface in parallel with the interfacial capacitance C_i. Interestingly, two semicircles are clearly observed in the Nyquist plots when the thickness of the copolymer film increases, i.e. for n >2 for (**poly-ZnT$_2$isoP$^{\bullet}$**) and n>10 for (**poly-ZnT$_2$P**). The emergence of the second impedance loop is attributed to the charge transport processes within the copolymer film. In this case,

the impedance spectra can be modelled with the equivalent circuit displayed in Figure 14 where R_{ct_film} is a charge transfer resistance in the film, C_f the chemical capacitance of the film and Z_w the Warburg impedance.

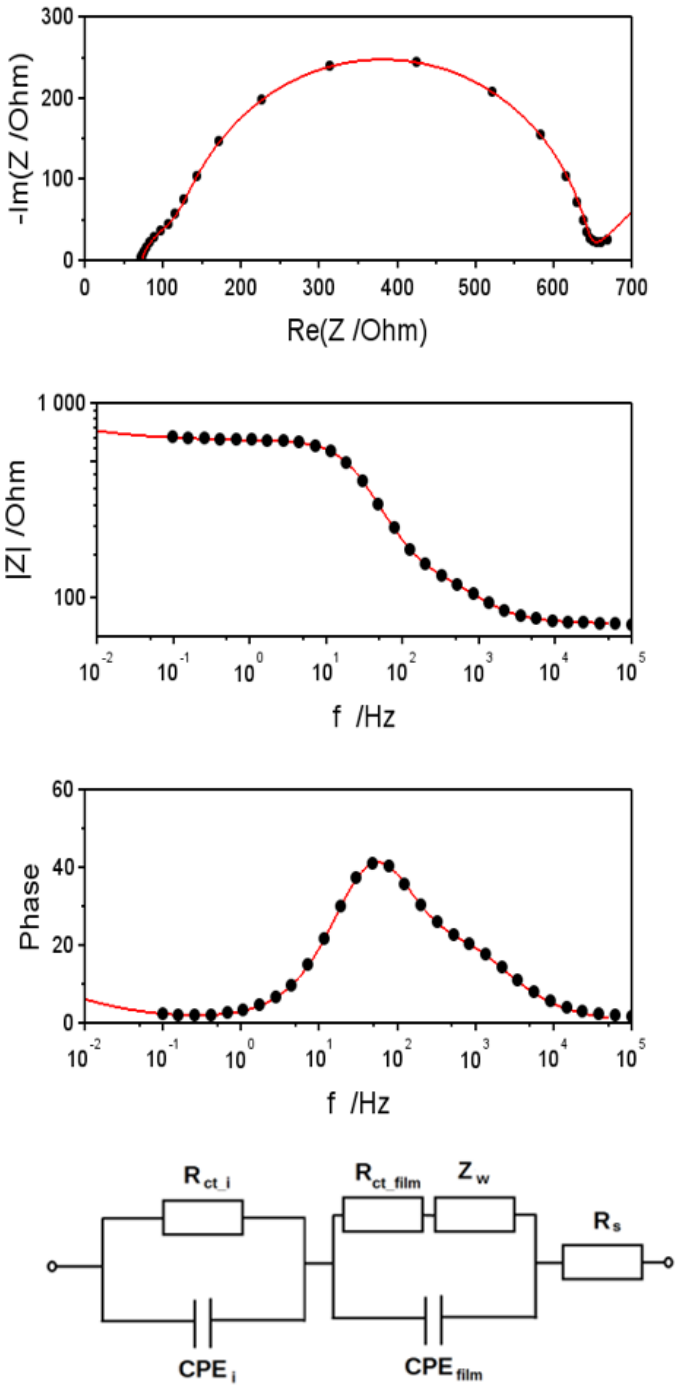

Fig. 14. Electrochemical impedance spectroscopy (EIS) Nyquist and Bode plots (phase *vs.* frequency (f) and |Z| *vs.* f) of **poly-ZnT$_2$isoP$^\bullet$** (n = 10). Measurements have been done in H_2O containing I_3^- 5 mmol L^{-1} and I^- 0.5 mol L^{-1}. BIAS potential: 0.00 V *vs.* OCP. Bottom: equivalent circuit used to fit the experimental data.

The evolution of R_{ct} and R_{ct_film} values as a function of n can be estimated from the fit of the experimental impedance spectra and is displayed in Figure 15B for the **poly-ZnT$_2$isoP$^\bullet$** and **poly-ZnT$_2$P** copolymers thin films. Overall, the charge transfer resistance R_{ct} at the ITO/copolymer interface decreases when n increases while the charge transfer resistance R_{ct_film} increases with the amount of copolymer deposited. For the **poly-ZnT$_2$isoP$^\bullet$** copolymer, R_{ct} ITO/copolymer decreases from ca. 20 kΩ for n=1 to ca. R_{ct} ~ 500 Ω for n=10, confirming the enhancement of the I^-/I_3^- charge transfer kinetics when the copolymer is present on the ITO. For n>10, R_{ct} reaches a plateau suggesting that the ITO surface is fully covered by the copolymer.

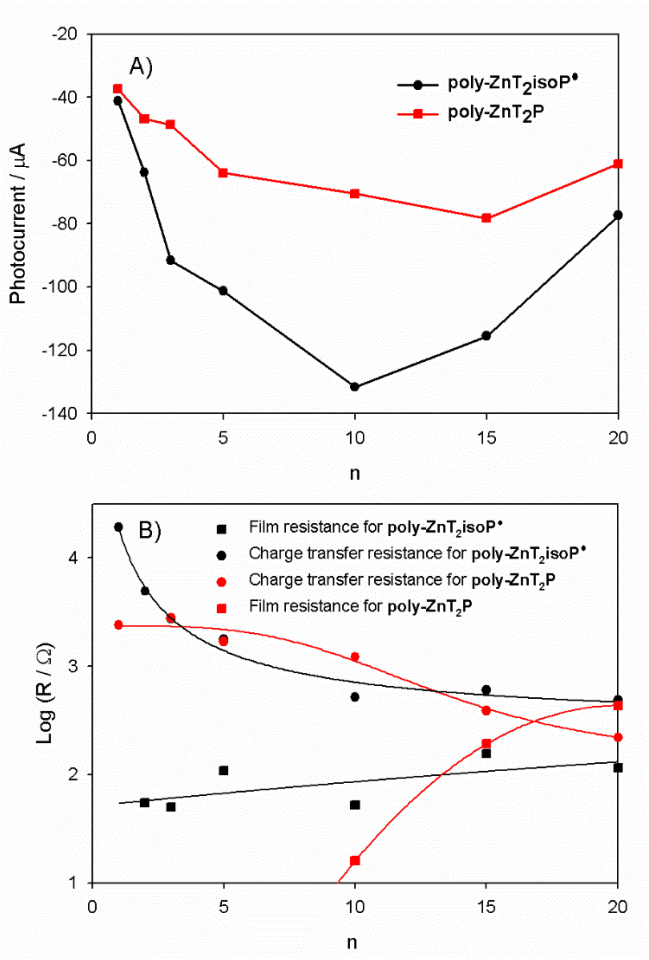

Fig. 15. A) Photoelectrochemical response of **poly-ZnT$_2$isoP$^\bullet$** (black line) and **poly-ZnT$_2$P** (red line) obtained with bpy^{++}–$(CH_2)_3$–$^+$bpy $2PF_6^-$ and **ZnT$_2$P** obtained with n = 1, 2, 3, 5, 10, 15 and 20 iterative scans. B) Plot of the Log(R) versus n (number of iterative scan,v = 100 mVs^{-1}, between -1.0 V and +1.0 V for **poly-ZnT$_2$isoP$^\bullet$** and between -1.0 V and +1.6 V for **poly-ZnT$_2$P**).
Measurements have been performed in H_2O containing I_3^- 5 mmol L^{-1} and I^- 0.5 mol L^{-1} under ~~one-off~~ light illumination from a 300W Xe arc lamp (with λ > 385 nm long pass filter). BIAS potential: 0.00 V *vs.* OCP. (For interpretation of the references to color in the figure legend, the reader is referred to the Web version of this article.)

Thus the enhancement of the photocurrent generation with the amount of deposited copolymer ~~that is~~ observed for n<10 might be attributed to the improvement ~~kinetics~~ of interfacial charge transfer kinetics and to the increase of the light harvesting efficiency of the film (Fig. 15A). For n>10, the charge transfer resistance within the film R_{ct_film} starts to increase reaching 100 Ω and 500 Ω at n=20 for the **poly-ZnT$_2$isoP$^{\bullet}$** and **poly-ZnT$_2$P** copolymers, respectively. The decrease of the photocurrent for n>10 stems from the slow kinetics of the charge transfer within the polymer films.

4. Conclusions

In summary, two porphyrin copolymer films have been prepared by the electro-oxidation of 5,15-ditolylporphyrin (**ZnT$_2$P**) in the presence of dipyridyl ligand 1,1''-(1,3-propanediyl)bis-4,4'-bipyridinium hexaflurophosphate salt ($(bpy^{+}–(CH_2)_3–^{+}bpy\cdot 2PF_6^{-}$). Electrogenerated radical cation porphyrin is a powerful electrophile which can rapidly react to form copolymer containing stable isoporphyrins (**poly-ZnT$_2$isoP$^{\bullet}$**). The existence of the π-cation radical of the isoporphyrin was proved by electron spin resonance spectroscopy. Further oxidation of **poly-ZnT$_2$isoP$^{\bullet}$** at higher applied potential forms a porphyrin containing copolymer (**poly-ZnT$_2$P**) with double viologen spacers. The electropolymerization process was scrutinized by EQCM. The achieved copolymers were characterized by UV-Vis-NIR spectroscopy, X-ray photoelectron spectroscopy, electrochemical impedance spectroscopy and AFM.

Mechanisms of electrochemical routes to these two types of electroactive copolymers have been discussed as well as the description of the unusual redox properties of copolymers containing stable isoporphyrin radicals.

The photocurrent measurements under visible-NIR light irradiation show that **poly-ZnT$_2$isoP$^{\bullet}$** thin films exhibit significantly enhanced performance in comparison to **poly-ZnT$_2$P**. However, the photovoltaic performances reach an optimum depending on the number of electropolymerization scans. The best performances are obtained for n =10 or 15. From electrochemical impedance spectroscopy measurements, it is observed that the charge transfer resistance of the film increases for films obtained with more than ten scans, thus explaining the decrease of photocurrent for films with n>10. Therefore, the control of the thickness of the copolymer films is of great importance to optimize the generation

of photocurrent under visible illumination. The overall conversion efficiency η of the sealed cell remains to be studied and measured.

Poly-ZnT$_2$isoP$^\bullet$ in the solid state could be stored for over several months and even one year without any degradation under ambient conditions in air. The stability is still good in DMF solution. Further investigations are underway in order to understand more about this remarkable stability. Other type of stable isoporphyrin radical are in preparation in our laboratory using various type of dipyridyl spacers "py-R-py". The reactivity is very dependent on steric hindrance of the porphyrin as well as the dipyridyl spacer and experimental conditions. Dipyridyl spacers with or without possible conjugation, with or without significant steric hindrance, with long, medium or short distance between the pyridyl groups will be synthesized and tested. Electrosynthesis of various isoporphyrin dimers will be also explored.

Acknowledgements

We thank CNRS, the Université de Strasbourg (France) and Université Pierre et Marie Curie (Paris, France) for funding of this work. LR also thanks the Université de Strasbourg for Labex CSC (Chemistry of Complex Systems) which has also supported one part of this research. MB thanks the Ministry of Higher Education and Scientific Research of Algeria for financing this thesis. We also thank the China Scholarship Council for a PhD grant to YL. We also thank Vasiliki Papaefthimiou for XPS measurements.

Appendix A. Supplementary data

Supplementary data associated with this article can be found, in the online version, at http://dx.doi.org/.....

References

[1] J. P. Evans, F. Niemevz, G. Buldain, P. R. Ortiz de Montellano, Isoporphyrin Intermediate in Heme Oxygenase catalysis oxidation of α-phenylheme, J. Biol. Chem. 283 (2008) 19530-19539.

[2] K. M. Barkigia, M. W. Renner, H. Xie, K. M. Smith, J. Fajer, Structural consequences of porphyrin tautomerization. Molecular structure of a zinc isoporphyrin, J. Am. Chem. Soc.115 (1993) 7894-7895.

[3] R. B. Woodward, Synthèse totale des chlorophylles, Angew. Chem., 72 (1960) 651-662.

[4] R. B. Woodward, The total synthesis of chlorophyll, Pure Appl. Chem.2 (1961) 383-404.
[5] D. Dolphin, R. H. Felton, D. C. Borg, J. Fajer, J. Am. Chem. Soc. 92 (1970) 743-745.
[6] J. A. Guzinski, R. H. Felton, *meso*-tetraphenylmethoxyisoporphyriniron(III) chloride, J. Chem. Soc. Chem. Commun. (1973) 715–716.
[7] H. J. Shine, A. G. Padilla, S.-M. Wu, Ion radicals. 45. Reactions of zinc tetraphenylporphyrin cation radical perchlorate with nucleophiles, J. Org. Chem. 44 (1979) 4069–4075.
[8] A. Gold, W. Ivey, G. E. Toney, R. Sangaiah, Ferric Isoporphyrins from Hydroperoxide Oxidation of (tetraphenylporphinato) iron (III) Complexes, Inorg. Chem. 23 (1984) 2932–2935.
[9] E. S. Schmidt, T. C. Bruice, R. S. Brown, C. L. Wilkins, Oxidation of (tetraphenylporphyrin)chromium(III) chloride by styrene ozonide, Inorg. Chem. 25 (1986) 4799–4800.
[10] W. A. Lee, T. C. Bruice, Transfer of oxygen from percarboxylic acids and alkyl hydroperoxides to (meso-tetraphenylporphinato)cobalt(III) chloride, Inorg. Chem. 25 (1986) 131–135.
[11] A. Hinman, B. J. Pavelich, A. E. Kondo, S. Pons, Oxidative voltammetry of some tetraphenylporphyrins in the presence of nucleophiles leading to isoporphyrins, J. Electroanal. Chem. Interfacial Electrochem. 234 (1987) 145–162.
[12] Y. Takeda, S. Takahara, Y. Kobayashi, H. Misawa, H. Sakuragi, K. Tokumaru, Isoporphyrins. Near-Infrared Dyes with Noticeable Photochemical and Redox Properties, Chem. Lett. (1990) 2103–2106.
[13] H. Segawa, R. Azumi, T. Shimidzu, Direct hydroxylation at the meso position of gold(III) tetraphenylporphyrin by nucleophilic addition: novel hydroxyphlorin derivatives, J. Am. Chem. Soc. 114 (1992) 7564–7565.
[14] Z. Cong, T. Kurahashi, H. Fujii, Formation of Iron(III) *meso*-Chloro-isoporphyrin as a Reactive Chlorinating Agent from Oxoiron(IV) Porphyrin π-Cation Radical, J. Am. Chem. Soc. 134 (2012) 4469–4472.
[15] J. Bhuyan, Nucleophilic ring-opening of iron(III)-hydroxy-isoporphyrin, Dalton Trans. 45 (2016) 2694–2699.
[16] G. J. Abhilash, J. Bhuyan, P. Singh, S. Maji, K. Pal, S. Sarkar, $^{\bullet}NO_2$-Mediated meso-Hydroxylation of Iron(III) Porphyrin, Inorg. Chem. 48 (2009) 1790–1792.
[17] J. Bhuyan, S. Sarkar, Oxidative Degradation of Zinc Porphyrin in Comparison with Its Iron Analogue, Chem. Eur. J. 16 (2010) 10649–10652.
[18] P. Schweyen, M. Hoffmann, J. Krumsieck, B. Wolfram, X. Xie, M. Brçring, Metal-Assisted One-Pot Synthesis of Isoporphyrin Complexes, Angew. Chem. Int. Ed. 55 (2016) 10118 –10121.
[19] W. R. Fawcett, M. Fedurco, K. M. Smith, H. Xie, The electrochemistry of a stable Zn isoporphyrin, J. Electroanal. Chem. 354 (1993) 281-287.
[20] K. M. Kadish, R. K. Rhodes, Reactions of metalloporphyrin. pi. radicals. 2. Thin-layer spectroelectrochemistry of zinc tetraphenylporphyrin cation radicals and dications in the presence of nitrogenous bases, Inorg. Chem. 20 (1981) 2961-2966.
[21] K. M. Kadish, E. V. Caemelbecke, G. Royal, in The Porphyrin Handbook, ed. K. M. Kadish, K. M. Smith and R. Guilard, Elsevier, San Diego, CA, 2003, vol. 8, p. 1. d) A. Harriman, G. Porter, P. Walters, Photo-oxidation of metalloporphyrins in aqueous solution, J. Chem. Soc. Faraday Trans. 1, 79 (1983) 1335–1350.
[22] M.-C. Richoux, P. Neta, P. A. Christensen, A. Harriman, Formation and decay of zinc tetrakis (N-methyl-3-pyridyl)porphine π-radical cation in water, J. Chem. Soc. Faraday Trans. 2 1986, 82, 235–249.
[23] W. Szulbiński, J. W. Strojek, Photo- and electrooxidation of water-soluble magnesium meso-tetraanilinporphyrin: Part 1. Photoinduced reduction of water to hydrogen, J. Electroanal. Chem. Interfacial Electrochem. 252 (1988) 323–334.

[24] S. Mosseri, J. C. Mialocq, B. Perly, P. Hambright, Porphyrins-cyclodextrin. 1. Photooxidation of zinc tetrakis(4-sulfonatophenyl)porphyrin (ZnTSPP) in cyclodextrin cavities: the characterization of ZnTSPP dication. Photolysis, radiolysis, and NMR studies, J. Phys. Chem. 95 (1991) 2196–2203.
[25] R. Guilard, N. Jagerovic, A. Tabard, C. Naillon, K. M. Kadish, Synthesis, spectroscopic and electrochemical characterization of different isomer types in tetrazolatoindium(III) porphyrins, J. Chem. Soc. Dalton Trans. (1992) 1957–1966.
[26] S. Gentemann, S. H. Leung, K. M. Smith, J. Fajer, D. Holten, Photophysical consequence of porphyrin tautomerization. Steady-state and time-resolved spectral investigations of a zinc porphyrin, J. Phys. Chem. 99 (1995) 4330 –4334.
[27] S. C. Mwakwari, H. Wang, T. J. Jensen, M. Vicente, H. Graça, K. M. Smith, Syntheses, properties and cellular studies of metallo-isoporphyrins, J. Porphyrins Phthalocyanines, 15 (2011) 918–929.
[28] J. Bhuyan, Metalloisoporphyrins: from synthesis to applications, Dalton Trans. 44 (2015) 15742–15756.
[29] A. Giraudeau, L. Ruhlmann, L. El-Kahef, M. Gross, Electrosynthesis and characterization of symmetrical and unsymmetrical linear porphyrin dimers and their precursor monomers, J. Am. Chem. Soc. 118 (1996) 2969.
[30] E. C. Johnson and D. Dolphin, The reactions of magnesium octaethylporphyrin and its Π-cations with nitrogen dioxide and nitrite, Tetrahedron Lett. 26 (1976) 2197-2200.
[31] L. Gong and D. Dolphin, Nitrooctaethylporphyrins: synthesis, optical and redox properties, Can. J. Chem. 63 (1985) 401-405.
[32] H. Xie and K. M. Smith, Stable isoporphyrin chromophores: synthesis, Tetrahedron Lett., 1992, 33, 1197-1200.
[33] P. Schweyen, M. Hoffmann, J. Krumsieck, B. Wolfram, X. Xie, M. Bröring, Metal-assisted one-pot synthesis of isoporphyrin complexes, Angew. Chem. Int. Ed. 55 (2016) 10118 –10121.
[34] T. Ogawa, Y. Nishimoto, N. Yoshida, N. Ono, A. Osukua, A. One-pot electrochemical formation of meso,meso-linked porphyrin arrays, Chem. Commun. (1998) 337–338.
[35] T. Ogawa, Y. Nishimoto, N. Yoshida, N. Ono, A. Osuka, Completely Regioselective Synthesis of Directly Linked meso,meso and meso,β porphyrin dimers by one-pot electrochemical oxidation of metalloporphyrins, Angew. Chem. Int. Ed. 38 (2004) 176–179.
[36] A. K. D. Dime, C. H. Devillers, H. Cattey, B. Habermeyer, D. Lucas, Control over the oxidative reactivity of metalloporphyrins. Efficient electrosynthesis of meso,meso-linked zinc porphyrin dimer, Dalton Trans. 41 (2012) 929–936.
[37] N. Yoshida, N. Aratani, A. Osuka, Poly(zinc(II)-5,15-porphyrinylene) from silver(I)-promoted oxidation of zinc(II)-5,15-diarylporphyrins, Chem. Commun. (2000) 197–198.
[38] C. H. Devillers, D. Lucas, A. K. D. Dime, Y. Rousselin, Y. Mugnier, Exploring the redox reactivity of magnesium porphine. Insight into the origins of electropolymerisation, Dalton Trans. 39 (2012) 2404–2411.
[39] O.I. Istakova, D.V., Konev, A.S. Zyubin, C.H. Devillers, M. A. Vorotyntsev, Electrochemical route to Co(II) polyporphine, J. Solid State Electrochem. 20 (2016) 3189-3197.
[40] D.V. Konev, O.I. Istakova, O. A. Sereda, M. A. Shamraeva, C.H. Devillers, M. A. Vorotyntsev, In situ UV-visible spectroelectrochemistry in the course of oxidative monomer electrolysis, Electrochimica Acta, 179 (2015) 315-325.
[41] S.D. Rolle, C.H. Devillers, S. Fournier, O. Heintz, H. Gibault, D. Lucas, A glassy carbon electrode modified by a triply-fused-like Co(II) polyporphine and its ability for sulphite oxidation and detection, New J. Chem. 42 (2018) 8180-8189.

[42] S.D. Rolle, D.V., Konev, C.H., Devillers, K.V. Lizgina, D. Lucas, C. Stern, F. Herbst, O. Heintz, M. A. Vorotyntsev, Efficient synthesis of a new electroactive polymer of Co(II) porphine by in-situ replacement of Mg(II) inside Mg(II) polyporphine film, Electrochemica Acta, 204 (2016) 276-2860.
[43] D.V. Konev, C.H. Devillers, K.V. Lizgina, V.E. Baulin, M. A. Vorotyntsev, Electropolymerization of non-substituted Mg(II) porphine: Effects of proton acceptor addition, J. Electroanal. Chem. 737 (2015) 235-242.
[44] M. A. Vorotyntsev, D.V. Konev, C.H. Devillers, I. Bezverkhyy, O. Heintz, Electroactive polymeric material with condensed structure on the basis of magnesium(II) polyporphine, Electrochimica Acta, 2011, 56, 3436-3442.
[45] M. A. Vorotyntsev, D.V. Konev, C.H. Devillers, I. Bezverkhyy, O. Heintz, Magnesium(II) polyporphine: The first electron-conducting polymer with directly linked unsubstituted porphyrin units obtained by electrooxidation at a very low potential, Electrochimica Acta, 22 (2010) 6703-6714.
[46] C.H. Devillers, D. Lucas, A/K/D/ Dime, K. D. Abdou, Y. Rousselin, Y. Mugnier, Exploring the redox reactivity of magnesium porphine. Insight into the origins of electropolymerisation, Dalton Trans. 39 (2010) 2404-2411.
[47] D. Schaming, L. Ruhlmann, Polyoxometalates Associated with Porphyrins used as Efficient Visible Photosensitizers; Trends in polyoxometalate research, Publisher Nova, Editors: L. Ruhlmann and D. Schaming, 2015, pp 237-264.
[48] D. Schaming, L. Ruhlmann, Electrosynthesis of oligo- and polyporphyrins based on oxidative coupling of Macrocycles, chapter in the book Electrochemistry of MN4 Macrocyclic Complexes, Springer, Zagal, J.H., Bedioui, Fethi, Dodelet, J.P. (Eds.). Vol 2, Biomimesis, electroanalysis, and electrosynthesis of MN4 metal complexes, 2016, pp 395-432.
[49] L. Ruhlmann, S. Lobstein, M. Gross, A. Giraudeau, An electrosynthetic path towards pentaporphyrins, J. Org. Chem. 64 (1999) 1352-1355.
[50] D. Schaming, Y. Xia, R. Thouvenot, L. Ruhlmann, An original electrochemical pathway for the synthesis of porphyrin oligomers, Chem. Eur. J. 19 (2013) 1712–1719.
[51] D. Schaming, S.M. Poullain, I. Ahmed, R. Farha, M. Goldmann, J.P. Gisselbrecht, L. Ruhlmann, Electrosynthesis and electrochemical properties of porphyrin dimers with pyridinium as bridging spacer, New J .Chem.35 (2011) 2534–2543.
[52] Z. Huo, A. Bonnefont, R. Farha, M. Goldmann, E. Saint-Aman, H. Xu, C. Bucher, L Ruhlmann, Photovoltaic properties of supramolecular assemblies obtained by incorporation of Preysler's type polyoxometalate in a polycationic copolymer of porphyrin, Electrochimica Acta, 274 (2018) 177-191.
[53] L. Ruhlmann, A. Giraudeau, One-pot electrochemical generation of a porphyrin dimer with bis(diphenylphosphonium)acetylene bridge, J. Chem. Soc., Chem. Comm. (1996) 2007-2008.
[54] L. Ruhlmann, A. Giraudeau, A first series of diphosphonium electrochemically bridged porphyrins, Eur. J. Inorg. Chem. (2001) 659-668.
[55] L. Ruhlmann, M. Gross, A. Giraudeau, Bisporphyrins with bischlorin features obtained by direct anodic coupling of porphyrins, Chem. Eur. J. 9 (2003) 5085-5096.
[56] C. H. Devillers, A. K. D. Dime, H. Cattey, D. Lucas, Electrochemical meso-functionalization of magnesium(II) porphine, Chem. Commun. 47 (2011) 1893–1895.
[57] L. Ruhlmann, A. Schulz, A. Giraudeau, C. Messerschmidt, J.-H. Fuhrhop, A Polycationic Zinc-5,15-dichlorooctaethylporphyrinate-viologen Wire, J. Am. Chem. Soc., 121 (1999) 6664-6667.
[58] L. Ruhlmann, J. Hao, Z. Ping, A. Giraudeau, Self-oriented Polycationic copolymers obtained from bipyrinium meso-substituted-octaethylporphyrins ,J. Electroanal. Chem. 621 (2008) 22-30.

[59] D. Schaming, J. Hao, V. Alain, R. Farha, M. Goldmann, H. Xu, A. Giraudeau, P. Audebert, L. Ruhlmann, Easy methods for the electropolymerization of porphyrins based on the oxidation of the macrocycles, Electrochimica Acta., 56 (2011) 10454-10463.
[60] Z. Huo, J.-P. Gisselbrecht, R. Farha, M. Goldmann, E. Saint-Aman, C. Bucher, L. Ruhlmann, Alternating electro-copolymerization of zinc-β-octaethylporphyrin with a flexible bipyridinium, Electrochimica Acta, 122 (2014) 108-117.
[61] R. Kannappan, C. Bucher, E. Saint-Aman, J.-C. Moutet, A. Milet, M. Oltean, E. Métay, S. Pellet-Rosaing, M. Lemaire, C. Chaix, Viologen-based redox-switchable anion-binding receptors, New J. Chem., 2010, 34, 1373-1386.
[62] A. Iordache, M. Retegan, F. Thomas, G. Royal, E. Saint-Aman, C. Bucher, Redox-responsive porphyrin-based molecular tweezers, Chem. Eur. J. 18 (2012) 7648-7653.
[63] J. S. Manka, D. S. Lawrence, High yield synthesis of 5,15-diarylporphyrins, Tetrahedron Lett. 30 (1989) 6989–6992.
[64] b) T. Takanami, M. Hayashi, H. Chijimatsu, W. Inoue, K. Suda, Palladium-Catalyzed Cyanation of Porphyrins Utilizing Cyanoethylzinc Bromide as an Efficient Cyanide Ion Source, Org. Lett. 7 (2005) 3937–3940.
[65] B. Habermeyer, A. Takai, C. P. Gros, M. El Ojaimi, J.-M. Barbe, S. Fukuzumi, Dynamics of Closure of Zinc Bis-Porphyrin Molecular Tweezers with Copper(II) Ions and Electron Transfer, Chem. Eur. J. 17 (2011) 10670–10681.
[66] C. Brückner, J. J. Posakony, C. K. Johnson, R. W. Boyle, B. R. James, D. Dolphin, Novel and improved syntheses of 5,15-diphenylporphyrin and its dipyrrolic precursors, J. Porphyrins Phthalocyanines.2 (1998) 455–465.
[67] M.O. Senge, Y. M. Shaker, M. Pintea, C.Ryppa, S. S. Hatscher, A. Ryan, Y. Sergeeva, Synthesis of meso-Substituted ABCD-Type Porphyrins by Functionalization Reactions, Eur. J. Org. Chem. 2 (2010) 237-258.
[68] S. Stoll, A. Schweiger, EasySpin, a comprehensive software package for spectral simulation and analysis in EPR, J. Magn. Reson. 178 (2006) 42-55.
[69] I. Azcarate, I. Ahmed, R. Farha, M. Goldmann, X. Wang, H. Xu, et al., Synthesis and characterization of conjugated Dawson-type polyoxometalate-porphyrin copolymers, Dalton Trans. 42 (2013) 12688–12698.
[70] A. Giraudeau, D. Schaming, J. Hao, R. Farha, M. Goldmann, L. Ruhlmann, A simple way for the electropolymerization of porphyrins, J. Electroanal. Chem. 638 (2010) 70-75.
[71] D. Schaming, I. Ahmed, J. Hao, V. Alain-Rizzo, R. Farha, M. Goldmann, H. Xu, A. Giraudeau, P. Audebert and L. Ruhlmann, Easy methods for the electropolymerization of porphyrins based on the oxidation of the macrocycles, Electrochim. Acta, 26 (2011) 10454–10463.
[72] A. Giraudeau, L. Ruhlmann, L. El-Kahef, M. Gross, Electrosynthesis and characterization of symmetrical and unsymmetrical linear porphyrin dimers and their precursor monomers, J. Am. Chem. Soc. 1996, 118, 2969.
[73] A. Giraudeau, S. Lobstein, L. Ruhlmann, D. Melamed, K.M. Barkigia, J. Fajer, Electrosynthesis electrochemistry, and crystal structure of the tetracationic Zn-meso-tetrapyridiniumyl-β–octaethylporphyrin, J. Porphyrins Phthalocyanines, 5 (2001) 793–797.
[74] C.H. Devillers, A.K.D. Dime, H. Cattey, D. Lucas, Electrochemical meso-functionalization of magnesium(II) porphine, Chem. Comm. 47 (2011) 1893-1895.
[75] A.K.D. Dime, H. Cattey, D. Lucas, C. H. Devillers, Electrosynthesis and X-ray Crystallographic Structure of Zn-II meso-triaryltriphenylphosphonium porphyrin and structural comparison with Mg-II meso-triphenylphosphonium porphine, Eur. J. Inorg. Chem. 44 (2018) 4834-4841.

[76] M. Berthelot, G. Hoffmann, A. Bousfiha, J. Echaubard, J. Roger, H. Cattey, A. Romieu, D. Lucas, P. Fleurat-Lessard, C. H. Devillers, Oxidative C-N fusion of pyridinyl-substituted porphyrins, Chem. Comm. 54 (2018) 5414-5417.
[77] T. Ogawa, Y. Nishimoto, N. Yoshida, N. Ono, A. Osukua, One-pot electrochemical formation of meso, meso-linked porphyrin arrays, Chem. Commun. (1998) 337–338.
[78] T. Ogawa, Y. Nishimoto, N. Yoshida, N. Ono, A. Osukua, Completely regioselective synthesis of directly linked meso meso and meso, β porphyrin dimers by one-pot electrochemical oxidation of metalloporphyrins, Angew. Chem. Int. Ed., 38 (1999) 176–179.
[79] A.K.D. Dime, C.H. Devillers, H. Cattey, B. Habermeyer, D. Lucas, Control over the oxidative reactivity of metalloporphyrins. Efficient electrosynthesis of meso, meso-linked zinc porphyrin dimer, Dalton Trans. 41 (2012) 929–936.
[80] S. Bruckenstein, M. Shay, Experimental aspects of use of the quartz crystal microbalance in solution, Electrochim. Acta, 30 (1985) 1295-1300.
[81] J. Fajer, Structural effects in chemistry and biology, J. Porphyrins Phthalocyanines, 2000, 4: 382–390.
[82] J.A. Shelnutt, X. Song J.G. Ma, S.L. Jia, W. Jentzen, C.J. Medforth Nonplanar porphyrins and their significance in proteins, Chem. Soc. Rev. 27 (1998) 31–42.
[83] K.M. Barkigia, M.D. Berber, J. Fajer, C.J. Medforth, M.W. Renner, K.M. Smith, Nonplanar porphyrins. X-ray structures of (2,3,7,8,12,13,17,18-octaethyl- and -octamethyl-5,10,15,20-tetraphenylporphinato)zinc(II), J. Am. Chem. Soc. 112 (1990) 8851–8857.
[84] L.D. Sparks, C.J. Medforth, M.S. Park, J.R. Chamberlain, M.R. Ondrias, M.O. Senge, K.M. Smith, J.A. Shelnutt, Metal dependence of the nonplanar distortion of octaalkyltetraphenylporphyrins, J. Am. Chem. Soc, 115 (1993) 581–592.
[85] M.O. Senge, M.W. Renner, W.W. Kalisch, J. Fajer, Molecular structure of (5,10,15,20-tetrabutyl-2,3,7,8,12,13,17,18-octaethylporphyrinato)nickel(II)—correlation of nonplanarity with frontier orbital shifts, J Chem Soc Dalton Trans. (2000) 381–385.
[86] F. D'Souza, M.E. Zandler, P. Tagliatesta, Z. Ou, J. Shao, C.E. Van Caemelbecke, K. M. Kadish, Electronic, Spectral, and Electrochemical Properties of (TPPBr$_x$)Zn Where TPPBr$_x$ Is the Dianion of β-Brominated-Pyrrole Tetraphenylporphyrin and x Varies from 0 to 8, Inorg. Chem. 37 (1998) 4567–4572.
[87] M.E. Anderson, A.G.M. Barrett, B.M. Hoffman, Super-Charged Porphyrazines: Synthesis and Physical Properties of Octacationic Tetraazaporphyrins, Inorg. Chem. 38 (1999) 6143–6151.
[88] C. Bernard, J.P. Gisselbrecht, M. Gross, E. Vogel, M. Lausmann, Redox Properties of Porphycenes and Metalloporphycenes. A Comparison with Porphyrins, Inorg Chem. 33 (1994) 2393–2401.
[89] M. Kasha, Relation between exciton bands and conduction bands in molecular lamellar systems, Rev. Mod. Phys. 1959, 31, 162-169.
[90] J.L. Sessler, M.R. Johnson, S.E. Creager, J.C. Fettinger, J.A. Ibers, Synthesis and characterization of quinone-substituted octaalkyl porphyrin monomers and dimers, J. Am. Chem. Soc. 112 (1990) 9310-9329.
[91] C. Inisan, J. Y. Saillard, R. Guilard, A. Tabard, Y. Le Mest, Electrooxidation of porphyrin free bases: fate of the π-cation radical, New J. Chem. (1998) 823-830.
[92] S. Breuer, D. T Pham, S. Huemann, K. Gentz, C. Zoerlein, R. Hunger, K. Wandelt, P. Broekmann, Organic layers at metal/electrolyte interfaces: molecular structure and reactivity of viologen monolayers, New Journal of Physics 10 (2008) 125033.
[93] Q. Wang, J.E. Moser, M. Grätzel, Electrochemical impedance spectroscopic analysis of dye-sensitized solar cells, J. Phys. Chem. B 109 (2005) 14945-14953.

[94] F. Fabregat-Santiago, J. Bisquert, G. Garcia-Belmonte, G. Boschloo, A. Hagfeldt, Influence of electrolyte in transport and recombination in dye sensitized solar cells studied by impedance spectroscopy, Sol. Energy Mater. Sol. Cells 87 (2005) 117e131.
[95] M. Adachi, M. Sakamoto, J. Jiu, Y. Ogata, S. Isoda, Determination of parameters of electron transport in dye-sensitized solar cells using electrochemical impedance spectroscopy, J. Phys. Chem. B 110 (2006) 13872e13880.